DOKUZ EYLÜL UNIVERSITY

GRADUATE SCHOOL OF NATURAL AND APPLIED SCIENCES

FRACTURES BEHAVIOR OF WELDED STEEL STRUCTURES SUBJECTED TO DYNAMIC LOADS

by

Seda GÜNEY

September, 2008

İZMİR

FRACTURES BEHAVIOR OF WELDED STEEL STRUCTURES SUBJECTED TO DYNAMIC LOADS

A Thesis Submitted to the
Graduate School of Natural and Applied Sciences of Dokuz Eylül University
In Partial Fulfillment of the Requirements for the Degree of Master of Science in
Mechanical Engineering, Mechanic Program

by

Seda GÜNEY

September, 2008

İZMİR

M.Sc THESIS EXAMINATION RESULT FORM

We have read the thesis entitled **"FRACTURE BEHAVIOR OF WELDED STEEL STRUCTURES SUBJECTED TO DYNAMIC LOADS"** completed by **SEDA GÜNEY** under supervision of **ASSISTANT PROFESSOR BİNNUR GÖREN KIRAL** and we certify that in our opinion it is fully adequate, in scope and in quality, as a thesis for the degree of Master of Science.

Assistant Professor Binnur GÖREN KIRAL

Supervisor

(Jury Member)

(Jury Member)

Prof. Dr. Cahit HELVACI

Director Graduate School of Natural and Applied Sciences

ACKNOWLEDGEMENTS

I am grateful to my supervisor Assist. Prof. Dr. Binnur GÖREN KIRAL for her support and continuous encouragement during this study.

I would also like to my family and my lovely friends for their encouragement and moral support.

I would also like to my colleague Didem KURT and my friend Ahmet YİĞİT for their continuous supporting.

SEDA GÜNEY

İzmir, 2008

FRACTURE BEHAVIOR OF WELDED STEEL STRUCTURES SUBJECTED TO DYNAMIC LOADS

ABSTRACT

The Marmara earthquake on August 17, 1999 resulted in great human tragedy for the Turkish people. Thousands of people died in the collapse of concrete building although steel structures, which are generally used for industry, could withstand. However, the Kobe in Japan (1995, January 17) and Northridge in US (1994, January 17) earthquakes brought about serious damage to some steel welded structures by unexpected failure in a brittle manner. This indicates that it is not only enough to use the steel structures in seismic areas but also necessary that they have ability of the connection to deform plastically without brittle fracture during an earthquake.

The goal of this thesis is to investigate and develop the performance of the steel welded connections. To this end, the effects of the material properties of the weld which is used in steel structures, crack placed in the weld region and dynamic loading on the fracture behavior of the structure have been examined. ABAQUS 6.5 has been used to examine the stress distribution in the welded steel structure and fracture behavior. Elastic and elasto-plastic finite element analyses have been performed. The nonlinear finite element analyses have been repeated for various frequency values of different loading cases in order to see the effect of the strain rate, which defines the earthquake loads. It is concluded that electrode type affects the fracture behavior of the welded structure.

Keywords : Fracture, finite element method, welded steel connections.

DİNAMİK YÜKLERE MARUZ KAYNAKLI ÇELİK BAĞLANTILARIN KIRILMA DAVRANIŞI

ÖZ

17 Ağustos 1999 tarihinde meydana gelen Marmara depremi Türk halkı için büyük bir insanlık dramına neden oldu. Binlerce insan tamamen çöken betonarme binalarda hayatını kaybederken aynı bölgede sanayi binaları için kullanılan çelik yapılar ayakta kalabildi. Ancak, Kobe-Japonya' da (17 Ocak, 1995) ve Northridge-ABD' deki (17 Ocak, 1994) depremlerin sonucunda kaynaklı çelik yapıların bazılarında meydana gelen beklenmeyen gevrek kırılmalar ciddi hasarlara neden oldu. Bu durum, deprem bölgelerinde sadece çelik yapı kullanmanın yeterli olmadığını, ayrıca bu yapıların bir deprem anında gevrek kırılmaya meydan vermeyecek uygun plastik deformasyon kapasitesinde bağlantıya da sahip olmaları gerektiğini göstermiştir.

Bu tezin amacı, kaynaklı çelik yapı bağlantılarının performansını incelemek ve arttırmaktır. Bunun için, çelik yapılarda kullanılan kaynağın malzeme özellikleri, kaynak bölgesinde yer alan çatlağın ve dinamik yüklemenin kırılma davranışına etkileri incelenmiştir. Kaynaklı çelik yapıda oluşan gerilme dağılımını ve kırılma davranışını incelemek için ABAQUS 6.5 programı kullanılmıştır. Elastik ve elasto-plastik sonlu elemanlar analizleri yapılmıştır. Deprem yükünü ifade eden şekil değiştirme hızının etkilerini görebilmek için nonlineer sonlu eleman analizleri çeşitli frekans değerlerindeki yükleme durumları için tekrarlanmıştır. Sonuç olarak, elektrot tipinin kaynaklı yapının kırılma davranışını etkilediği görülmüştür.

Anahtar Kelimeler : Kırılma, sonlu elemanlar yöntemi, kaynaklı çelik bağlantılar.

CONTENTS

Page

CHAPTER ONE
INTRODUCTION

The 7.4 magnitude Marmara earthquake of August 17, 1999 was a devastating catastrophe and thousands of people died in the collapse of numerous concrete buildings. The predominant structural system used for buildings in Turkey consists of reinforced concrete frames with unreinforced masonry infills. Nevertheless, it is not enough simply to use steel structures in a seismic area to avoid damage due to earthquake. The Northridge (1994, January 17) and Kobe (1995, January 17) earthquakes brought about serious damage to some welded steel structures, whose supposedly ductile connections unexpectedly failed in a brittle manner.

That earth-shattering event provided both a perplexing problem and the motivation for researchers to establish improvements in the engineering of welded steel structures (Toyoda, 2001). According to much research reviewing the fracture behavior which occurred during the Kobe earthquake, the key reasons why brittle fracture occurred were both the "large cyclic and dynamic straining" during the heavy earthquake and the existence of poor design and fabrication (Toyoda, 2001). In the 1995 Kobe earthquake, some of the welded box type steel columns in a steel constructed expressway were crushed in compression, under the high level of vertical ground acceleration. This was due to the brittle fracture of the welds causing the four sides of the box column to separate into four independent plates. This is reminiscent of the brittle fracture of the welded joints in steel frame buildings in the Northridge earthquake in 1994. In the Kobe earthquake, steel buildings were also observed to have suffered relatively significant damage (Scawthorn 2000). Seismic engineering design theory relies either on isolation of the structure or on the ability of a rigid frame to deform plastically in an earthquake without fracture. When this failed to occur in both the American and Japanese events, much debate ensued over the causes and solutions. Research and investigation in both countries have resulted in a number of changes to building codes and specifications (IIW, 2002).

Most of the damage to steel moment frames in the Northridge earthquake occurred at the typical welded flange-bolted web connection detail. The beam flanges had been field welded to the columns using single bevel complete penetration groove welds with backing bars. The majority of fractures occurred at the bottom flange of the beams, with a much smaller number at the beam top flanges. Weld root flaws were often present, that extended from the backing bar notch deeper into the weld. However, the low toughness weld metal obtained by using the electrodes designated as E70T-4 and by high deposition rate welding procedures, and possibly indifferent inspection, failed to detect flaws which appear to have played an important role in inducing brittle fractures (IIW, 2002).

Extensive studies have been carried out to develop ductile beam-to-column connection details for the use in seismic areas.

Matos and Dodds (2001) developed and applied a probabilistic model to study the dynamic, nonlinear fracture behavior in the beam lower-flange to column welds found in moment resistant steel frames. The effort focused on connection designs used prior to the 1994 Northridge earthquake. They applied the same probabilistic model to examine and compare fracture behavior in the simpler pull-plate specimen developed after the Northridge event to simulate conditions at the lower-flange connection.

Matos and Dodds (2001) studied on an advanced micro-mechanics model of cleavage fracture in ferritic steels to examine the nonlinear fracture behavior of welded, moment resistant steel frames of the type widely constructed prior to the 1994 Northridge earthquake. They used 3-D finite element analyses, coupled with an advanced micro-mechanics fracture model based on the Weibull stress to assess the relative significance of loading rate, residual stresses, plasticity, access hole geometry, beam yield strengths, and various weld (backup bar) modifications. A probabilistic model was developed to study the dynamic, nonlinear fracture behavior in the beam lower-flange to column welds.

Nakagomi et al. (1997) examined the relation between the design, execution of work, and the brittle fracture of the beam-end welded connection. They investigated the influence, which the efficiency of structural steel and the weld metal exerts on the fracturing of a welded connection.

Fracture analyses were carried out for fractured steel structures observed from the Kobe and Northridge earthquakes and from full-scale model tests by Shimanuki et al. (1998). They considered the effects of the small defects, high strain rate cyclic loading, and large plastic deformation on the fracture of seismic damaged steel structures. The fracture mechanics methods discussed was based on the CTOD design curve approach by taking into account the effects of the plastic constraint, dynamic and cyclic large deformation.

Fisher et al. (1998) discussed the test methods for measuring fracture toughness as well as the Charpy V-Notch toughness required to minimize the potential for brittle fracture. They explained fracture mechanics analysis, which predicted that brittle fracture would occur in welded steel moment frame connections before yielding.

Xue et al. (1996) studied of two follow-up tests on the full-scale moment connections to investigate the effects of the weld metal toughness on the ductile performance. Of the two specimens, one is a fully welded connection fabricated with E70TG-K2 flux cored electrode and the other is a connection that was previously tested to failure (weld fracture) and subsequently repaired by replacing the cracked E70T-4 welds with E7018 weld metal, which has specified minimum notch toughness.

Finite element analysis was performed to determine the distribution of stresses in beam-to-column connections when subjected to sway loading as would arise under earthquake loading by Burdekin et al. (1998). Allen et al. (1998) also made analytical and experimental studies to evaluate the stress, strain and force distributions in welded steel moment frames.

Toyoda (1997) studied on the strain rate effect on the fracture behaviors of steel framed structures. He tested smooth bars and the notch specimens. The 3-D static and dynamic finite element analyses were performed to examine the strain rate effect on the characteristic near-tip stress field.

Azuma et al. (2000) investigated beam-to-column connections with weld defects tested under cyclic loads and evaluated the fracture toughness properties of numerically modeled weld defects.

Kuntiyawichai and Burdekin (2003) studied the effects of dynamic loading on both fracture toughness specimens under rapid loads and cracked connections in steel framed structures under earthquake loads using the finite element method.

Righiniotis et al. (2002) simplified two-dimensional crack model for assessing the fracture of bottom flange welds in steel beam-to-column connections and presented the formulation of the approximate expressions for the stress intensity factors related to the cracked geometry accounting for typical stress conditions.

Shi and Sun (1997) aimed to extend the knowledge of the effect of weld width on the J-integral crack driving force and then to investigate the influence of weld width on the R6 failure assessment diagram. They considered the interaction of weld strength mismatch and crack depth, to the weld width.

Lei and Ainsworth (1997) estimated the J integral by using an equivalent stress-strain relationship approach for three-point-bend specimens containing a weld with mismatched mechanical properties. Elastic-plastic finite element analyses were performed to verify this approach.

Thaulow et al. (1997) investigated the stress fields for a crack located at the fusion line of a weldment. The strength mis-matching and the size of the heat affected zone were varied and the corresponding distribution of the maximum principle stress was examined.

Shi et al. (1998) examined the effects of weld strength mismatching and geometry parameters on the relationship between J-integral and the crack tip opening displacement (CTOD). Numerical analyses were carried out by an ABAQUS two-dimensional elastic-plastic analysis mode.

Xiao and Dexter (1998) calculated the applied J-integral as a function of applied displacement for cracked full-scale test specimens, which are representative of ship structural components using the finite element analysis.

Nakagomi et al. (1998) studied on the beam-to-column connection considering mechanical property of the structural steel and weld material. They tested to see the effects of the toughness of structural steel and weld metal on the plastic deformation capacity and the behavior of fracture of the specimen.

Paterson et al. (1998) examined the materials of construction of welded steel beam-to-column connection, its controlling material properties, the possible variation in the material properties, and the corresponding structural integrity.

The aim of this thesis is an assessment of the safety of the welded beam-to-column connections under static and dynamic loadings in order to avoid the brittle fracture. The effects of the weld material and dynamic loading on the J-integral and stress distribution in the weld joints are examined. Numerical analyses are carried out by ABAQUS three-dimensional elastic-plastic analysis mode. In order to examine the effects of the strain rate and mechanical properties of the weld material on the fracture behavior of the beam-to-column connection, a simplified three-dimensional solid model is modeled and semi-elliptical surface crack is placed through the heat-affected zone at the connection where the column flange meets the bottom flange of the beam.

CHAPTER TWO
PROBLEM DEFINITION

2.1 Introduction

The design theory of seismic engineering is based either on isolation of the structures or on the ability of a rigid frame to deform plastically in an earthquake without fracture. Research and investigation in recent post earthquake have resulted in a number of changes to building codes and specifications. Changes were introduced to the widely used UBC Code (Uniform Building Code) in 1997. An extensive and comprehensive series of investigations and reports has been completed in the USA by the SAC Joint Venture under contract to the Federal Emergency Management Agency (FEMA). Extensive investigations have also been carried out in Japan and New Zealand leading to the production of Japanese Recommendations, the Comite International pour le Develloppement et l' Etude de la Construction Tubulaire (CIDECT) recommendations and a New Zealand Standard. General guidance on design of steel buildings for seismic loading has been developed in Eurocode 8 (IIW, 2002).

The International Institute of Welding (IIW) promulgated the international perspectives on welding-related issues. In 1996, Commission XV on the Fundamentals of Design and Fabrication for Welding formed a Sub-commission, XV-G, to conduct further investigation into this issue. As a result of discussion with Commission X on Fracture Avoidance, a Joint Working Group was created consisting of both Commission members. The result of their efforts was the creation of these Recommendations.

Controlling fracture should not be interpreted as absolute prevention of fracture, but as the most reasonable technical means to reduce the risk of occurrence and the extent and type of brittle fracture. The inherent nature of structures subject to repeated high strain low cycle fatigue loading makes it very unlikely that onset of some cracking can be completely avoided. However, the objective should be that,

while fracture initiation may occur even under the best of circumstances, fracture propagation should be limited and of a non-life-threatening nature. Accordingly, neither the engineer nor the client should anticipate a cost-free seismic survival event, even if the earthquake is of the so-called "moderate" variety. Some expense will always be incurred in rehabilitating a post-event structure that has been subject to an earthquake severe enough to generally disrupt the functioning of society in that location. The nature and extent of such rehabilitation will be a political, technical and economic decision and based as much on a perception of safety as on the actual threat of crack propagation.

Decisions on the complex issues concerned with avoidance of fracture in welded moment frame connections require the engineers to be competent and knowledgeable in a number of fields. It is unlikely that such knowledge will be found in a single person and hence it is likely that it will be necessary to bring together a team of specialists covering the following fields:

- Structural design for seismic conditions
- Material selection for strength, weldability and fracture resistance
- Fracture mechanics procedures
- Fabrication and welding technology
- Inspection and non destructive testing

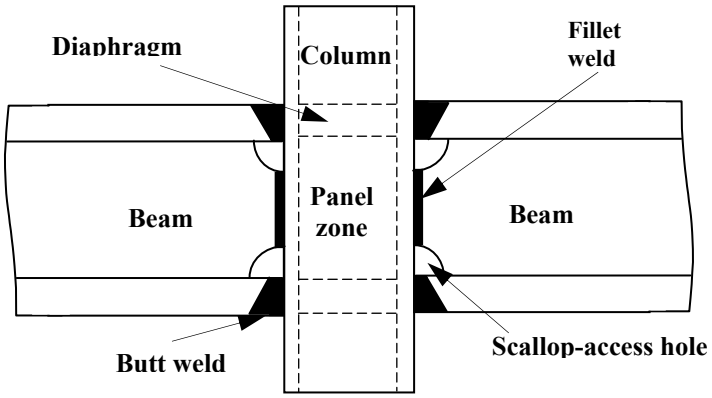

Figure 2.1 Beam-to-column connection

2.2 Experiences from Northridge and Kobe Earthquakes

The vast majority of damage to steel moment frames in the Northridge earthquake occurred at the typical welded flange-bolted connection detail. The beam flanges were field welded to the column using single bevel complete penetration groove welds with backing bars. The majority of fractures occurred at the beam bottom flanges, with a much smaller number at the beam top flanges. Weld root flaws were often present that extended from the backing bar notch deeper into the weld. However, low toughness weld metal obtained by using the electrodes designated as E70T–4 and by high deposition rate, welding procedures and possibly indifferent inspection failing to detect flaws appear to have played an important role in inducing brittle fractures.

More than 90 per cent of steel multi-storey building frames in Japan use box-section columns and connections which have through-flange continuity plates, also called through diaphragms. The beam flanges are field-welded to the through diaphragms using single bevel complete penetration groove welds with backing bars. Cracks frequently started at toes of weld access holes prepared in the beam webs or at weld toes of groove welds around the weld tab regions (the starting and stopping ends of welded butt joints) and extended in a brittle manner across the beam flanges during the Kobe earthquake.

One of the reasons for frequent occurrences of fracture in this area is that the lack of flexural capacity in the bolted web connection leads to over-stress of the beam flange and the flange groove welds. If the web bolts slip, the bolted web-connection requires relatively large deformation in order to develop significant flexural capacity. Therefore, much stiffer flange welds resist most of the bending moment and a significant proportion of shear at a connection. This tendency is even more pronounced when a rectangular hollow section (RHS) column is used, as the shear tab is welded onto the more flexible thin-walled column flange. One important difference in damage pattern between the US and Japanese events is that at Northridge fracture occurred with little visible sign of yielding of material in regions

where cracks started, while in Kobe most cracks started with ductile tears which changed to brittle fracture after plate elements in connections sustained extensive yielding or local buckling. Consequently, improvements of connection design proposed in the two countries appear somewhat contrasting. In the USA, connection details should demonstrate, by approved cyclic testing results or calculation, the ability to meet their overstrength requirements (ICBO 1997), while in Japan no emergency change of the building code was undertaken.

Extensive investigations have been performed both in the US and Japan to find improved details for avoidance of premature tensile failure of beam-to-column connections. The results of these investigations are summarised in the SAC Reports and Guidelines, Recommendations for the Design of Connections of Steel Structures, the Japanese Welding Engineering Society Report on Method for Assessment of Brittle Fracture (WES TR 2808) and the CIDECT Design Guide (IIW, 2002).

2.3 Basic Principles for Earthquake Resistant Structures

2.3.1 Design Issues

The major issues, which have to be taken into account in design of moment connections for seismically loaded steel structures, are the applied strain levels and strain rates, the effects of stress concentrations, the effects of welding in relation to the effects of flaws and of residual stresses, and the material property requirements in terms of strengths and fracture resistance.

2.3.1.1 Earthquake Load and Energy Dissipation Capacity

The existing seismic codes specify design earthquake loads as a function of the energy dissipation capacity of structures. Furthermore, all these codes specify detailing rules for structural elements and frames to ensure that the structure can dissipate a certain amount of energy.

Keeping an ordinary building structure nearly elastic to provide for the probability of such a rare occurrence as an earthquake is usually grossly uneconomical and not usually attempted unless the structure is isolated from ground shaking by using special devices. Base isolation is an option, which should be considered at the design stage for severe earthquake zones.

2.3.1.2 Dissipative and Non-Dissipative Structural Behaviors

Earthquake resistant designs of steel framed moment resisting structures are commonly based on one of the following two design concepts:

a) Dissipative structural behavior
b) Non-dissipative structural behavior

In concept (a), the capability of parts of the structure (called dissipative zones) to resist earthquake loads beyond their elastic region is taken into account. Members and joints in dissipative zones sustain yielding or local buckling and participate in dissipating input energy during earthquakes by hysteretic behavior.

In concept (b), a frame analysis is based on an elastic analysis without taking into account nonlinear material behavior. For structures designed using concert b) the resistance of members and joints can be evaluated in accordance with the standard design rules for steel structures. The design concert b) may only be used for small minor structures or structures in low seismicity zones, slender trussed structures or isolated structures and will not be discussed any further in this document.

2.3.1.3 Structural Behavior of Moment Resisting Frames

Steel building frames resist horizontal earthquake loads by moment resisting frames or by braced frames. Moment resisting frames resist horizontal loads by members acting in an essentially flexural manner. In these structures, the dissipative

zones are mainly located in plastic hinges near the beam-column connections and energy is dissipated by means of cyclic inelastic bending.

2.3.1.4 Joints in Dissipative Zones

The following criteria can be defined for seismic design:

1. Structural parts of dissipative zones should have adequate ductility and resistance for the structure to sustain sufficient deformation without incurring overall instability of the structure.

2. Non-dissipative parts of lateral systems of dissipative structures and the connections of the dissipative parts to the rest of the structures should have sufficient over strength and stability to allow the cyclic yielding of the dissipative parts. Engineers need to be aware of moment magnification due to higher modes.

2.3.1.5 Strong Column-Weak Beam Design

The formation of hinges in columns, as opposed to beams, is generally undesirable, because this may result in the formation of a storey mechanism, in which damage concentrates on a few storeys and relatively few elements participate in energy dissipation. In addition, such a mechanism may result in local damage to the columns that are critical gravity load bearing elements.

Eurocode 8 states, “Moment resisting frames shall be designed so that plastic hinges form in the beams and not in the columns. This requirement is waived at the base of the frame, at the top floor of multi-storey buildings and for one storey buildings.” The SAC Design Criteria and the Japanese design guides recommend that, in order to avoid plastic hinges occurring in all the columns in a few storeys, the sum of plastic moment capacities of columns should be about 1.5 times greater than the sum of plastic moment capacities of beams at each connection. The value of 1.5 is the result of engineering judgements based on the examinations of several

influencing factors, including the variability of the yield strength in beam and column materials.

2.3.2 Brief Summary of Other Procedures

The Eurocode 8 document covers all aspects of design of earthquake resistant structures but only the aspects affecting the behavior of connections in moment resisting steel frames. It should be noted that Eurocode 8 requires the design of such frames to ensure that if plastic hinges occur, these take place in the beams, and that the connections should be stronger than either the beams or columns. This specification does not cover fracture requirements explicitly but refers to Eurocode 3 for general requirements.

The Japanese document WES TR 2808 gives details of a fracture mechanics treatment to assess fracture performance of steel structures under seismic loading. This uses an extended version of the Crack Tip Opening Displacement (CTOD) design curve developed for high strain conditions by the Japanese to determine a required toughness level to withstand the design loading. The results are expressed in terms of CTOD fracture toughness with a correlation to Charpy test requirements. The method does take account of the effects of plastic strain and high strain rate on the required Charpy properties and also includes a correction factor for effects of constraint. This document does not make specific recommendations for toughness and material properties but gives methods for assessing requirements in conjunction with information about stress/strain levels and flaw sizes.

The USA SAC/FEMA approach is the result of extensive and comprehensive research investigations and testing leading to prescriptive sets of requirements. Two types of frames are defined, Special Moment Frames (SMF) and Ordinary Moment Frames (OMF). SMF are designed to have higher ductility than OMF whereas OMF are intended to have higher strength but with less ductility available. Frames are required to have a capacity for ductility based on interstorey drift angle. The SAC/FEMA investigations define connections, which failed at ISD values less than

0.03 as having limited rotational capacity, whilst above ISD values of 0.03 connections showed significant rotational capacity. This is essentially the ultimate condition, and modified limits for strength degradation are adopted in Section 6 following the CIDECT recommendations. Welded unreinforced connections with a bolted web are pre-qualified only for OMF, whilst connections pre-qualified for SMF included welded unreinforced connections with welded webs, reduced beam flange sections, welded free flange connections and bolted end plate connections. Connections with additional cover plates or haunches are not included as pre-qualified because, in the view of SAC/FEMA, they do not offer significant advantages over other simpler and more cost effective alternatives. SAC/FEMA guidelines concentrate more on structural design detailing and on weld metal properties than on improved fracture toughness properties of the parent steel. There are a series of standard pre-qualified design details with associated material property and fabrication quality requirements. Although not derived from the likely loads and flaw dimensions which may be encountered, the requirements for Charpy impact energy or notch toughness for parent material are 20 ft-lbs at 70 ^{o}F whilst a combination of 40 ft-lbs at 70^{o}F and 20 ft-lbs at 0^{o}F is required for the weld metal. There are specific requirements concerning use and removal of backing strips and weld tabs and for the use of a profiled geometry weld access hole to give reduced stress concentration effects. Several issues/concerns have been identified by SEAOC (one of the organisations participating in SAC) in their review of FEMA 350 (SEAOC 2002).

The New Zealand HERA approach gives alternatives of selecting steels by a notch ductility method based on maximum thicknesses for different grade s based on Charpy test properties or a fracture mechanics method based on the use of BSI Document PD 6493 (now BS 7910). For seismic -applications the permissible minimum service temperature for different grades of steel is increased by 10 ^{o}C to allow for the reduced probability of seismic loading occurring at minimum temperature.

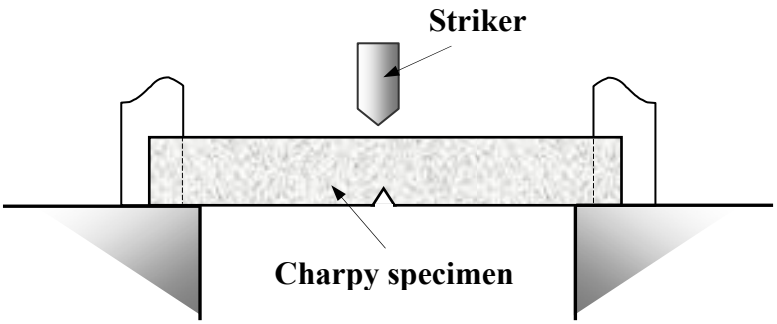

Figure 2.2 Charpy V-notched impact test

2.3.3 Material Issues

The selection of steel type and quality is vital for preventing brittle behavior of the material or welding at the minimum service temperature. The use of brittle material will render useless all other considerations as the element or connection will fail without any significant energy absorption. Amongst the detailed issues concerned with selection of materials are the following:

- Strengths of materials including yield to tensile ratio
- Base metal and HAZ toughness
- Deposited weld metal toughness
- Through thickness direction properties
- Ductility
- Effects of strain rate
- Effects of pre-straining during cyclic earthquake conditions (cyclic strain hardening)
- Material testing methods

To ensure sufficient overstrength of joints, Eurocode 8 suggests that the value of the yield strength of the steel actually used in the fabrication should not exceed by more than 10 % the specified minimum yield strength of the material used in the design.

The Japanese recommendations for assessment of brittle fracture (reference 9) make allowance for the effects of both plastic strain and high strain rates in determining fracture toughness requirements. These requirements are determined by fracture mechanics procedures based on developments of the Japanese WES 2805 methodology and use crack tip opening displacement (CTOD) as the measure of toughness with a correlation to Charpy test values.

2.3.4 Fabrication Issues

There have been extensive debates about the significance of various issues, which arise as part of considerations of details of fabrication. These include the following:

- Welder qualification and type of tests
- Welding procedure qualification/selection of welding parameters
- Welding processes
- Welding position
- Base metal preparation
- Overall welding and individual pass sequence, including max & min temperatures
- Stress concentrations/flaws due to fabrication (e.g. use of backing strips and weld tabs, access holes, lack of fusion, lack of penetration, undercut, misalignment)
- Quality control methods

The SAC/FEMA recommendations give detailed requirements for the removal of weld tabs and fusible backing strips and subsequent non-destructive testing for many types of joints. They also give detailed recommendations for a preferred design of access hole with controlled slope and radii to limit the stress concentration effect.

2.4 IIW Risk Assessment Procedures

The normal design procedure for moment-resisting steel framed buildings for seismic loading conditions involves sizing of the members such that the structure can dissipate the energy produced by the maximum accelerations anticipated for the magnitude of earthquake concerned. This requires the steel at the regions where energy dissipation is expected to take place to have sufficient ductility to withstand some degree of plastic strain and yielding. The structural designer has to assess the risk of the severity of earthquake, which may occur and then carry out an iterative procedure to assess the risk of failure or severe damage to the structure.

The selection of steel to prevent in-service brittle fracture requires assessment of the steel toughness level required for the structural loading and stress distribution in the various elements, presence of flaws or severe local stress concentrations, and the minimum service temperature. The normal method for specifying available fracture resistance of steels for general structural purposes uses the Charpy-V notch impact test, with different grades of steel characterised by the temperature at which minimum energy absorption is guaranteed. The most common value of this energy absorption is 27 Joules (20 ft-lbs), and commonly used temperatures for this minimum energy in different grades of steel are +20, 0, –20, –30, –40, –50 and –60 ^{o}C.

The two alternative Risk Assessment Procedures (RAPs) described below are designed to enable an engineer to assess qualitatively the risk of brittle fracture associated with material properties, the sizes of flaws present in welds and the level of stress/strain conditions that a building is designed to withstand. RAP 1 (Section 2.4.1) represents a simple and generally conservative method based primarily on practical experience from the Kobe and Northridge earthquakes whilst RAP 2 (Section 2.4.2) provides a more complex assessment of risk based on a series on analytical studies using a combination of finite element and fracture mechanics methods.

2.4.1 Simple Procedure – Level I

2.4.1.1 Material Selection Requirements

Research into the fractures, which occurred in the earthquakes at Northridge and Kobe, has suggested that risk of failure can be expressed in the ranges shown in Table 2.1, where the Charpy energy requirements are minima for weld metal, HAZ or base metal at the minimum service temperature at which an earthquake is considered likely to occur:

Table 2.1 Level l Assessment

Charpy Energy Absorption (J)	**Risk of brittle fracture in steel structure**
$C_v > 100$	Risk of brittle fracture very low
$47 < C_v < 100$	Low risk of fracture
$27 < C_v < 47$	Medium risk of fracture
$10 < C_v < 27$	High risk of fracture- stringent countermeasures essential
$C_v < 10$	Very high risk -structural base isolation/protection essential

These requirements can be adjusted to equivalent values at standard testing temperatures in steel supply specifications

2.4.1.2 Effect of Additional Factors

It will be noted that the above Table 2.1 gives guidance based only on Charpy energy and level of demand for plastic strain required for seismic energy absorption, expressed as cumulative rotation factor or inter storey drift. Experience of the behavior of structures in the earthquakes at Northridge and Kobe has shown the occurrence of fractures to be influenced by various controlling factors related to the four main fields: design, material, fabrication and inspection.

2.4.2 General Procedure - Level 2

In this approach, the degree of risk of fracture is assessed in terms of stress and strain levels at the joint; flaw sizes assessed in terms of the fabrication details and the NDT applied; and material toughness, as outlined below.

2.4.2.1 Stress and Strain Levels at the Joint

The demand for applied plastic strain levels experienced at a joint for a given earthquake can be expressed in terms of the joint rotation. This in turn depends on the interstorey drift angle produced at a particular location in a frame by the earthquake loading. The resistance of a joint to plastic deformation can be expressed by the ratio of the fully plastic moment capacity of the joint to that of the beam (M_{pj}/M_{pb}). It should be noted that this ratio must take account of the actual yield strength properties of the joint and beam and not just of the minimum specified properties. The following Table sets out the stress and strain conditions likely to be experienced in the welded regions of the joint for different combinations of interstorey drift/plastic rotation and ratio M_{pj}/M_{pb}.

2.4.2.2 Fabrication Details, Flaw Sizes and Non-Destructive Testing

The three categories, 1 → 3 in worsening order, suggested for fabrication details, NDT and permissible flaw sizes a_p are as follows:

1. Non-fused backing strip used, or fused backing strip removed with root back gouged and sealed, controlled welding procedures and qualified welders. Weld tabs used at ends of welds and removed after welding with ends ground flush. Access holes if used made to SAC/FEMA preferred detail or no access holes used at all, and NDT carried out using ultrasonic and magnetic testing with qualified operators and procedures to ensure that no detectable flaws remain. Maximum anticipated flaw height which might remain undetected = 3 mm.

2. Fused backing strip left in place with additional 6 mm leg length fillet weld between backing strip and column flange, controlled welding procedures and qualified welders. Weld tabs used at ends of welds and removed after welding with ends ground flush, or alternatively flux tabs used. Access holes made to normal construction standards and NDT carried out using ultrasonics. Max anticipated flaw height up to 0.15 times the flange thickness up to a maximum of 6 mm.

3. Fused backing strip left in place with no additional precautions, no special controls on weld tabs or access holes, no NDT carried out. Max anticipated flaw height up to 0.3 times flange thickness up to a maximum of 12 mm.

2.4.2.3 Toughness

The three categories 1 → 3 in worsening order, suggested for toughness are as follows, based on fracture mechanics analyses, where T_{min} is the minimum service temperature and T_{27} is the temperature for a minimum of 27 J energy absorption in the Charpy test for weld metal, heat affected zone and parent material:

1. Charpy test properties for beam, column section and weld metal satisfy the following requirement:

$$T_{min} - T_{27} > 40\ ^{o}C \quad \text{, or} \quad K_{mat} > 200\ \text{MPa}\sqrt{m}\text{,} \quad \text{or} \quad \delta_{mat} > 0.5\ \text{mm}$$

2. Charpy test properties for beam and column section and weld metal satisfy the following requirement:

$$40\ ^{o}C \geq T_{min} - T_{27} \geq 20\ ^{o}C \quad \text{, or} \quad 200 \geq K_{mat} \geq 140\ \text{MPa}\sqrt{m}\text{,} \quad \text{or} \quad 0.5 \geq \delta_{mat} \geq 0.25\ \text{mm}$$

3. No control on Charpy test properties for beam or column section, weld metal or heat affected zone. Properties expected to be of the order of those below:

$$20\ ^{o}C > T_{min} - T_{27} > 0\ ^{o}C \quad \text{, or} \quad 140 > K_{mat} > 100\ \text{MPa}\sqrt{m}\text{,} \quad \text{or} \quad 0.25 > \delta_{mat} > 0.15\ \text{mm}$$

2.5 Supporting Recommendations

2.5.1 Design Strengthening

It is clear that there is an overriding effect of the relative strengths of the beam, column and connection on the location of plastic hinges when energy dissipation is required. The strength of the connection should be greater than both the beam and the column and that the column should also be stronger than the beam. This arrangement should ensure that any plastic hinges will form in the beam and that no major demand for plasticity should occur in the welded connection (IIW, 2002).

Steel structures are anticipated to develop their ductility through the development of yielding in beam-to-column assemblies at the column-beam connections. This yielding may take the form of plastic hinging in the beams (or, less desirably, in the columns), plastic shear deformation in the column panel zones, or through a combination of these mechanisms (FEMA, 2000).

Observation of damage sustained by buildings in recent great earthquakes indicated that contrary to the intended behavior, in many cases, brittle fractures initiated within the connections at very low levels of plastic demand, and in some cases, while the structures remained essentially elastic. Typically, but not always, fractures initiated at the complete joint penetration weld between the beam bottom flange and column flange (Figure 2.3). Once initiated, these fractures progressed along a number of different paths depending on the individual joint conditions as shown in Figure 2.5 (FEMA, 2000, Matos & Dodds, 2001).

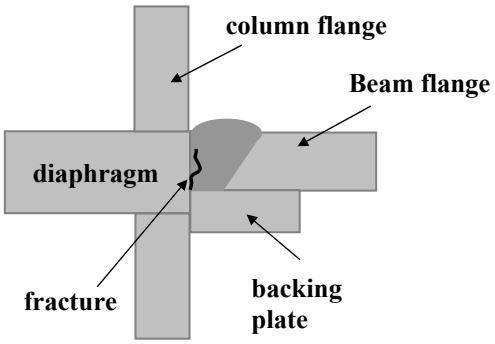

Figure 2.3 Common zone of fracture initiation in beam-to-column connection

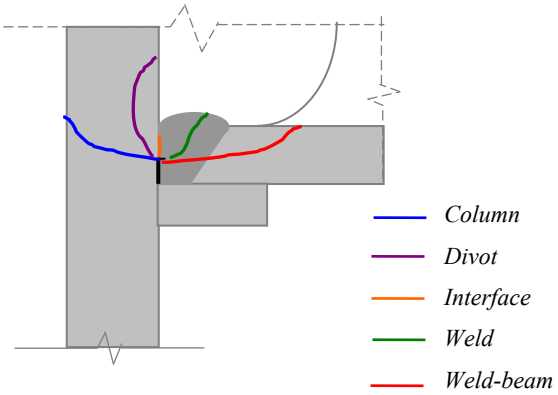

Figure 2.4 Paths for propagation of crack originating from root pass defects in the lower-flange weld

2.5.2 Base (Parent) Material Strength

The base metals should be specified with both minimum and maximum yield strengths to ensure that the design intent of relative strengths of column, beam and connection is achieved.

2.5.3 Weld Metal Strength

It is recommended that the yield strength of the weld metal should overmatch the actual strength of the parent material of the beam and column.

2.5.4 Charpy Testing (CVN)

The Charpy V-Notch impact test requirements given are minimum levels for deposited weld material, heat affected zone or base section or plate material at the minimum service temperature at which an earthquake is considered likely to occur. For the weld metal, Charpy specimens should be taken at the root of the weld from a weld procedure test welded to represent welding of the actual structural joints concerned. The specimens should be taken with their length perpendicular to the line of the weld and the line of the notch root should be perpendicular to the weld surfaces, commonly referred to as “through-thickness” notch orientation. For the heat affected zone the Charpy specimens should be taken nom the level of the weld with highest he at input and notched at the fusion line and at 2 mm nom the fusion line with the same orientation as the weld metal specimens. Base material Charpy properties may be obtained nom the supplier’ s test certificates but the possibility of carrying out check tests, particularly in the transverse direction should be considered.

2.5.5 Base Metal through Thickness Properties

Material properties for designs that load material normal to the rolled surface, i.e., through thickness loading, need to be considered in relation to the possibility of lamellar tearing. Properties in respect of ductility in the through thickness direction are typically less than longitudinal value s, depending on the presence of non-metallic inclusions such as manganese sulphides. For highly restrained joints involving transfer of forces in the through thickness direction and subject to high stress strain conditions, it is suggested that reduction of area values of 25% in through thickness direction tensile tests would be appropriate. This would be expected to be achieved if the sulphur content of the steel is kept below 0.010%.

2.5.6 Backing Strips

Backing strips are sometimes used on the underside or root of butt or groove welds to enable the whole of the weld to be made from the top side, in the downhand

or fiat position. They may be of the same material as the components being welded, (i.e. steel), in which cage they are fused to the underside of the weld. Alternatively, backing strips may be made of materials, which are not fused during welding - typical examples of these are copper or ceramic backing strips. Care should be taken if copper backing strips are used to ensure that no copper contamination has occurred to cause cracking or embrittlement in the weld root. If a backing strip is left fused to the underside of the weld, it causes a stress concentration in the root and it makes it more difficult to carry out non-destructive testing reliably. Many fractures occurred in structures in the Northridge earthquake initiating from defects associated with the root of the weld immediately adjacent to backing strips. This issue has received considerable attention in the SAC/FEMA recommendations where it is required that backing strips should be removed and the root of the weld sealed by welding with an additional 6mm (1/4 inch) leg fillet weld followed by ultrasonic testing to confirm freedom from defects.

2.5.7 Weld Tabs

Weld tabs are used at the ends of butt or groove welds to allow the weld to be carried past the ends and ensure that the full weld cross section is obtained over the length of the joint. It is difficult to ensure that the ends of the welds have the full cross section and are free from defects. If weld tabs are used and left in place, they will cause local stress concentrations, which may act as initiation positions for fracture. It is recommended that for critical butt or groove welded connections in steel structures, weld tabs should be used during welding. On completion of welding, the tabs should be removed by cutting off followed by dressing of the weld ends to match the profile of the parent material.

2.5.8 Welding Procedures

Welding of connections associated with steel structures should be carried out in accordance with written welding procedures for the type of joint and materials concerned. These procedures should specify the welding conditions (process,

position, current, are voltage, travel speed, heat input, preheat, maximum interpass temperature etc.) for each joint type in accordance with either the Contract Specification or with National Specifications as appropriate.

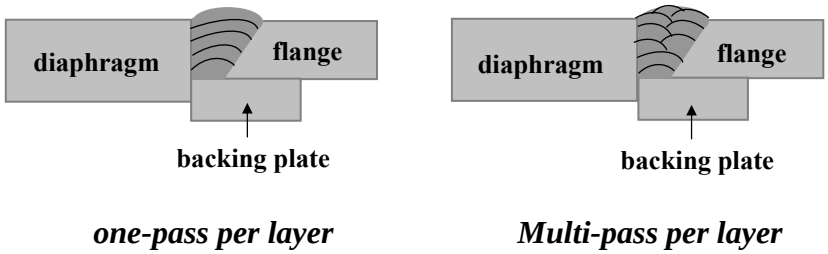

Figure 2.5 Welding pass sequence (Toyoda, 1998)

2.5.9 Welder Qualification

All welders employed on welding of connections associated with steel structures should be qualified for welding the type of connection concerned, using the welding process and procedures concerned, for materials and welding position concerned, by having completed appropriate welder qualification test pieces.

2.6 The Effects of the Dynamic Loading

Earthquakes are examples of dynamic loading which may cause serious structural damage and potential loss of life. The structural engineering earthquake design community was severely shocked by the effects of the earthquakes at Northridge, California in 1994 and at Kobe, Japan in 1995. There were widely spread connection fractures within welded steel moment resisting frames which were originally thought to have been designed to be strong enough to resist the stresses, and ductile enough to accommodate the distortions generated by a severe earthquake.

The influence of dynamic load on material behavior is often ignored in structural design. In reality, an inertia effect from dynamic load can cause plastic behavior. From the research work in the last forty years, it is known that increasing the loading

rate affects the material properties of steel. Normally, the quasi-static tests of yield stress f_y are conducted at low strain rates of about 10^{-3} s^{-1}. Under seismic loading conditions for short periods the local strain rates in structures may be excess of 10^{-1} s^{-1}, causing increases in f_y of 30%. Manjoine (1944) investigated the behavior of low-carbon steel under dynamic loading. He discovered that the lower yield stress and ultimate tensile stress increased with increasing strain rate (Kuntiyawichai & Burdekin, 2003).

The fracture toughness of structural steels normally increases with decreasing loading rate and increasing temperature. It can be assumed that loading rate is proportional to strain rate. This implies that the material cleavage fracture toughness decreases with increasing strain rate (Kuntiyawichai & Burdekin, 2003).

2.7 Full-scale Test

Numerous experiments were realized in order to verify the design criteria for beam-to-column connections under extreme seismic conditions by the researchers (Arimochi et al., 1998, Popov et al., 1985, Suita & Tada, 1998, Kauffman et al., 1997, Xue et al., 1996, Nakagomi et al., 1997, Kurobane, 1998, Nakagomi, 1998, Clifton et al., 1998, Scholz et al., 1998). As a result of these experiments, several design alternatives have been suggested as possible replacement candidates for the pre-earthquake connection. The test setup for steel welded connection is shown in Figure 2.6.

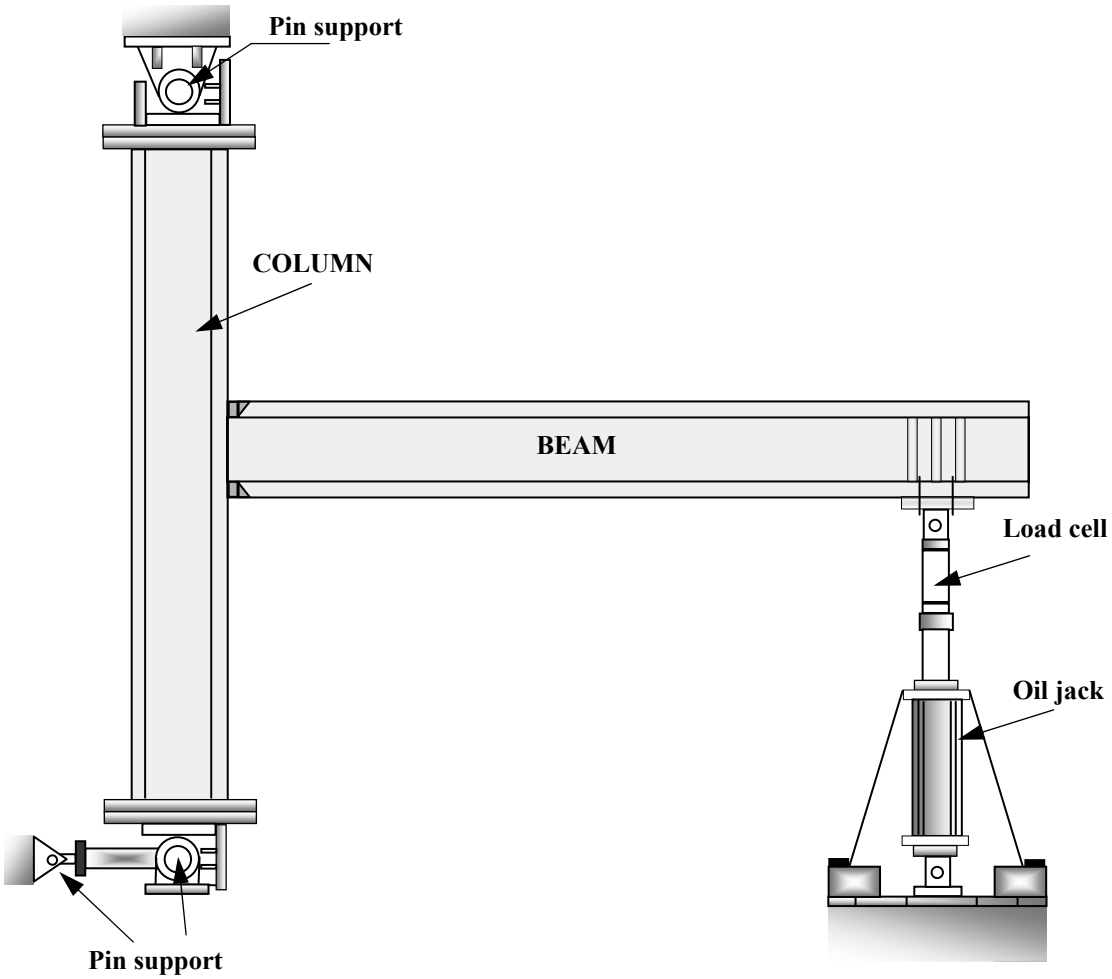

Figure 2.6 Full scale test setup (Suita & Tada, 1998)

Full-scale laboratory tests of these connections are quite expensive. Kauffman and Fisher developed the so-called “pull-plate” test specimen which isolates the fracture prone lower flange weld from other (geometric) parameters involved in the connection behavior. The pull-plate test enables rapid, more economical evaluation of alternative welding procedures. Static and high-rate tests performed on the pull-plate specimen revealed the same kind of failures found in full-scale connections. Axial loads applied to the pull-plate specimen do not impose a secondary (local) bending at the weld-column flange interface as predicted by models of the full connections due to the web access hole. This reduces constraint at crack fronts and must be addressed to transfer toughness values measured in the pull-plate specimens

to assess similar cracks in full connections. Additional tests in-progress using this specimen are investigating a broad range of welding procedures, backup bar designs and loading rates.

In this study, fracture behavior of the pull-plate specimen subjected to axial forces on cracks located in the lower-flange weld region is examined using 3-D finite element analyses. Figure 2.7 shows full-joint and the simplified pull-plate specimen.

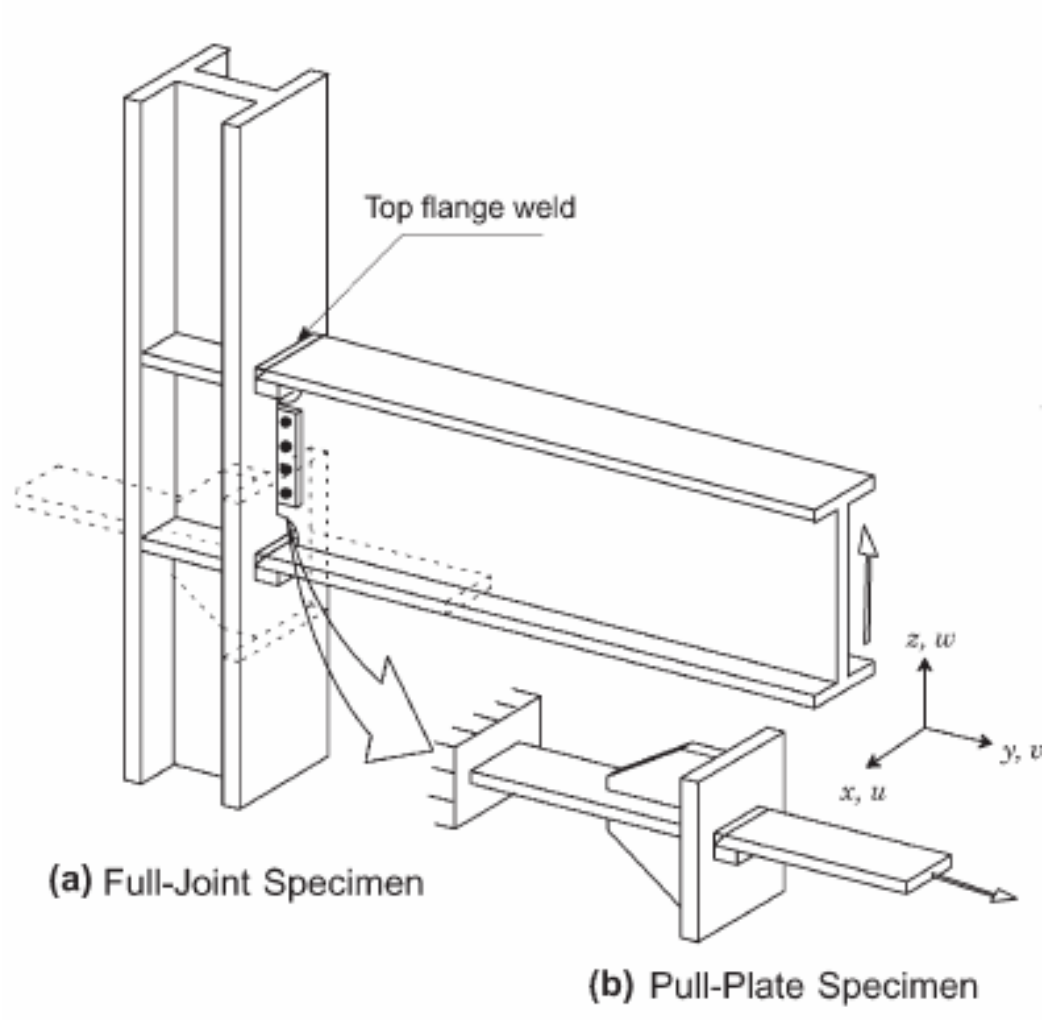

Figure 2.7 (a) Schematic of typical pre-Northridge beam-column connection. (b) The simplified pull-plate specimen (Matos & Dodds, 2001).

The pull-plate connections are investigated considering material properties of electrode and loading conditions. The static and dynamic elastic-plastic finite element analyses are performed. In the analyses, four different type electrodes are examined to compare the effects on the fracture behavior of the steel structures.

2.8.1 Material Properties

The materials of beam and column are both A 572 steel Gr. 50. E7018, E70TG-K2, E70T-6 and E71T-8 electrodes are used for the flange welds in order to see the effects of the electrode type. The mechanical properties of the materials used can be seen in Table 2.2.

As can be seen in the table, E70T-4 is a low toughness flux core electrode and commonly used in steel structures before the 1994 Northridge earthquake and it is not used in this study. E71T-8, E70T-6 and E70TG-K2 are notch-tough rated weld metals that are higher toughness. E7018 is extremely high toughness weld electrode (Chi, 1999).

Table 2.2 Material properties of base and weld metals (Chi, 1999)

Material	**CVN_s (J)**	**CVN_d (J)**	**K_{IC} (MPa√m)**	**$CTOD_c$ (mm)**
A572	266	266	252	0.47
E70T-4	54	14	85	0.045
E70T-6	68	50	100	0.041
E70TG-K2	120	98	120	0.078
E71T-8	250	109	140	0.114
E7018	197	185	204	0.307

To account for the dynamic loading effects in the CVN test, the temperature shift by +120 ^{o}F is necessary to convert the dynamic CVN values to the static CVN values (Barson et al., 1987, Chi, 1999).

Due to expense and size limitations associated with fracture toughness tests, it is useful to make estimations of fracture toughness from CVN toughness requirements. The empirical correlation between CVN and K_{IC}, fracture toughness, is as follows (Motarjemi & Koçak, 2002):

$$K_{IC} = \sqrt{\frac{E\left(0.53CVN^{1.28}\right)\times 0.2^{\left(0.133CVN^{0.256}\right)}}{1000\left(1-\upsilon^2\right)}}$$

where K_{IC} in MPa$\sqrt{\text{m}}$ and CVN in Joule.

K_{IC} can be also converted $CTOD_C$,

$$K_{mat} = \sqrt{m \cdot \sigma_{flow} E \cdot CTOD}$$

where for plane-strain problem m=1.6 (Broek, 1989) and $\sigma_{flow}=(\sigma_y+\sigma_u)/2$ is flow stress (Chi, 1999).

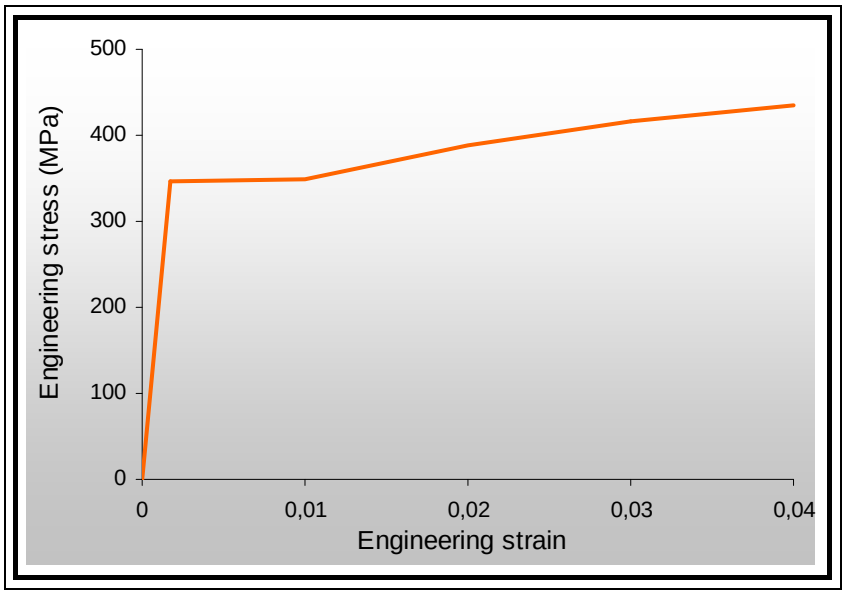

Figure 2.8 Stress-strain curve of base metal (A572)

Figures 2.8 and 2.9 show the stress-strain curves of the base and weld electrodes used in this study. Mechanical properties of A572 Gr. 50 steel plate and beam and column flanges material are also reported by Ricles (1999), Dexter (1999) and Dong (1999) (Chi, 1999, Dong, 1999).

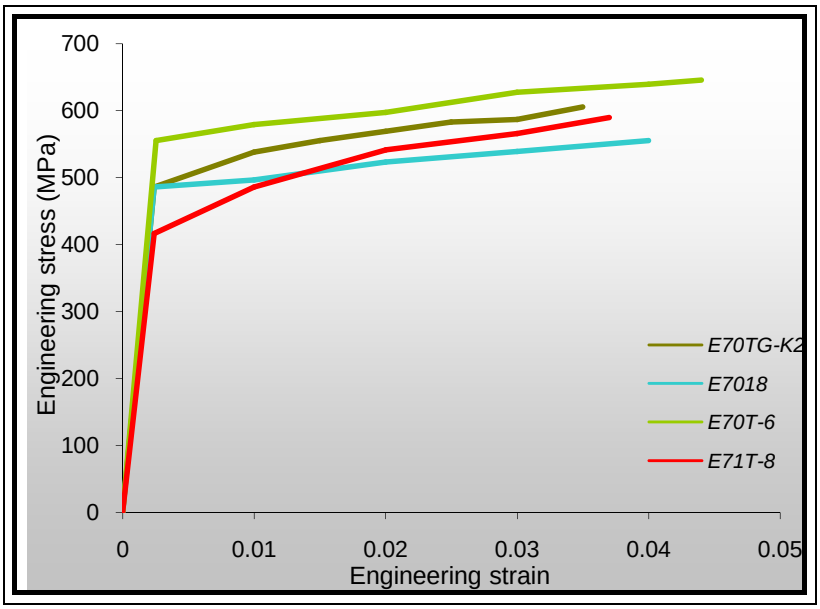

Figure 2.9 Stress-strain curves of weld metals

2.8.2 Crack Configuration

Most fractures initiated at the lower flange weld in the connections. Full-scale, laboratory tests of these type connections following the earthquake exhibited very similar fractures, now generally attributed to a combination of factors including mechanical and metallurgical defects created by manual, on-site welding; use of low-toughness electrodes; heavy plate thicknesses and high stresses; and the various geometric discontinuities.

The crack type chosen to represent the defect must be relatively close to real defects in structures. Therefore, the initial defect is modeled as a semi-elliptical surface crack (EC3, 1995). The crack is assumed to be planar. Furthermore, since the defect size is small compared to the size of a structural element, it is assumed that the

plate dimensions are infinite. The crack is defined by its length, *a*, and shape *a/c*, where is half crack surface width (AWS, 2000).

The length of the initial defect or crack is defined as follows. Cracks are detectable by inspections in shop both for thin and thick plates. However, defects tend to be greater in thicker plates and larger welds. A linear function would give too small values for small plate thicknesses to be detectable and too large values for thick plates which would result in exaggerated requirements. Therefore, as this was considered the best engineering approach, a logarithm function of the plate thickness was proposed

$$a=ln(t) \qquad \text{(AWS, 2000)}$$

In this thesis, semi-elliptical surface crack is placed through the heat-affected zone at the connection where the column flange meets the bottom flange of the beam as shown in Figure 2.7.

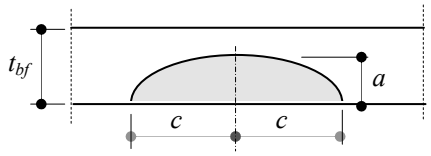

Figure 2.10 Geometry of the initial defect chosen a semi-elliptical surface crack in an infinite plate (AWS, 2000).

CHAPTER THREE
FRACTURE MECHANICS

3.1 Introduction

Fracture is a problem that society has faced for as long as there have been man-made structures. The problem may actually be worse today than in previous centuries, because more can go wrong in complex technological society.

The cause of most structural failures generally falls into one of the following categories:

1) Negligence during design, construction or operation of the structure.
2) Application of a new design or material, which produces an unexpected (and undesirable) result.

In the first instance, existing procedures are sufficient to avoid failure, but are not followed by one or more of the parties involved, deu to human error, ignorance, or willful misconduct. Poor workmanship, inappropriate or substandard materials, errors in stress analysis, and operator error are examples of where the appropriate technology and experience are available, but not applied.

The second type of failure is much more difficult to prevent. When an "improved" design is introduced, there are invariably factors that the designer does not anticipate. New materials can offer tremendous advantages, but also potential problems. Consequently, a new design or material should be placed into service only after extensive testing and analysis. Such an approach will reduce the frequency of failures, but not eliminate them entirely; there may be important factors that are overlooked during the testing and analysis.

3.2 The Fracture Process

Fracture is often considered as a process in which increased loading suddenly causes accelerated growth of a pre-existing crack. A closer study, however, reveals three distinct phases,

1) loading without crack growth
2) stable crack growth
3) un stable crack growth

Stable crack growth may, in principle, be controlled with the loading device, so that, for instance, a prescribed slow crack growth may be obtained. This is not possible for unstable crack growth, which occurs spontaneously.

Four distinctly different regions may be recognized in a crack edge vicinity. Nearest the edge is the *process region*. When the crack edge advances, a *wake of the process region* is left behind. Outside the process region there is generally a *plastic region*. When the crack edge advances a *wake of the plastic region* is left behind. In this wake the material is again deforming elastically, because of unloading, but reversed plastic flow may eventually occur, so that a *secondary plastic region* appears behind the wake of the *primary plastic region*. The process region and the primary and secondary plastic regions are the dissipative regions. Outside them is the elastic region. In Figure 3.1, the three phases of the fracture process are illustrated, together with the process region and the (primary) plastic region with its wake.

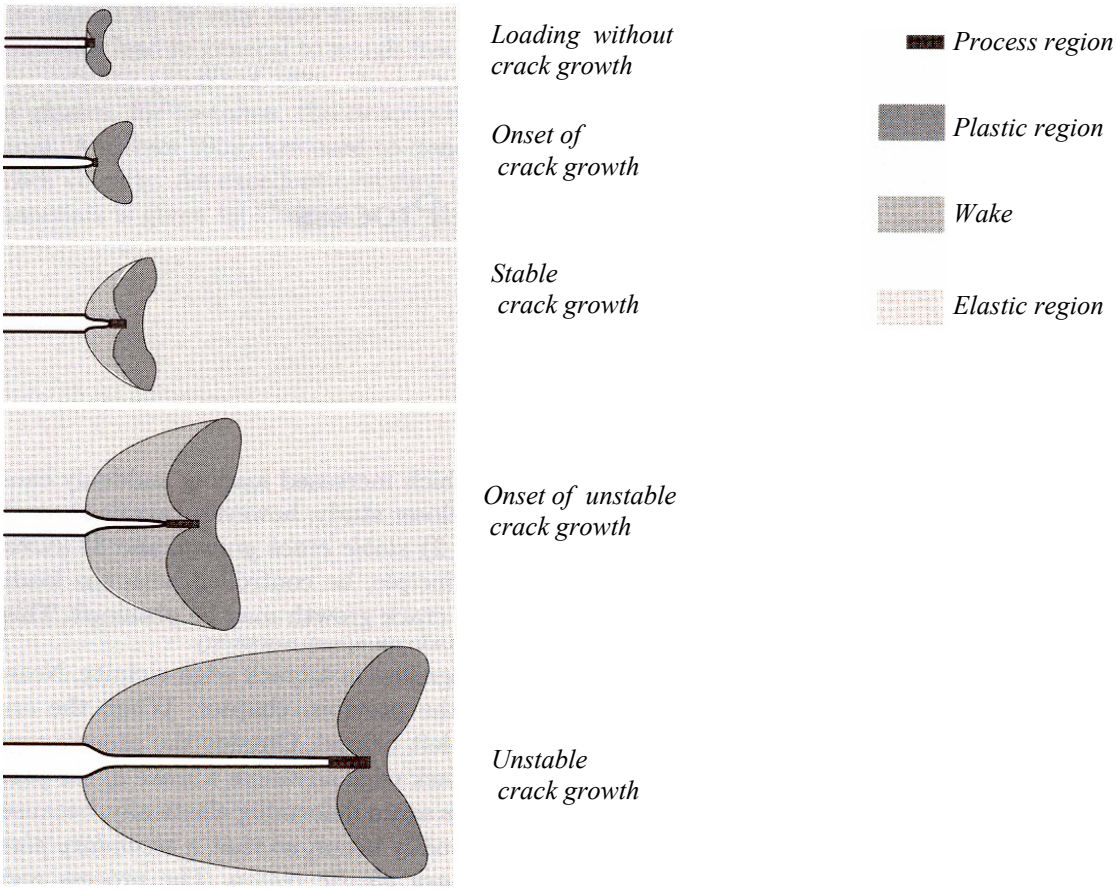

Figure 3.1 The phases of the fracture process are

3.2.1 Pre-existing Cracks

Pre-existing cracks are very common and virtually impossible to avoid in large structures. In some solids, for instance, glass, tiny surface cracks appear spontaneously because of chemical agents, even in seemingly neutral environments, such as air with normal humidity. In order cases, cracks are opened because of thermal stresses, created, for instance, after heat treatment (hardening) or welding. Cracks are also frequently formed during manufacturing or joining structural parts.

A pre-existing crack is generally not simply a sharp slot in a virgin material. Such a slot would be only a few inter-atomic distances wide, but pre-existing cracks in steels, for instance, may how openings of several hundred inter-atomic distances,

and sometimes much more. The material state in the crack edge vicinity varies considerably, depending on the history of crack formation. This variety calls a philosophy of handling fracture problems that does need to consider the previous history, which, moreover, is generally poorly known. On the other hand, it is desirable to know whether the mechanism that caused cracking is still present. It is, for example, important to recognize the existence of residual stresses that have caused cracks during or after welding.

3.3 Loading before Crack Growth

Suppose that a crack is so oriented that the ambient stresses tend to open it. Even a small load causes a separation of the crack faces, and a strain concentration appears at the crack edge(s). In most materials, plastic flow follows, and during further loading the strains or stresses become sufficiently high to initiate micro-separations: a process region develops. Continued increase of the load causes growth of both the process region and the plastic region. Eventually, coalescences occur between micro-separations and the main crack: the crack starts growing.

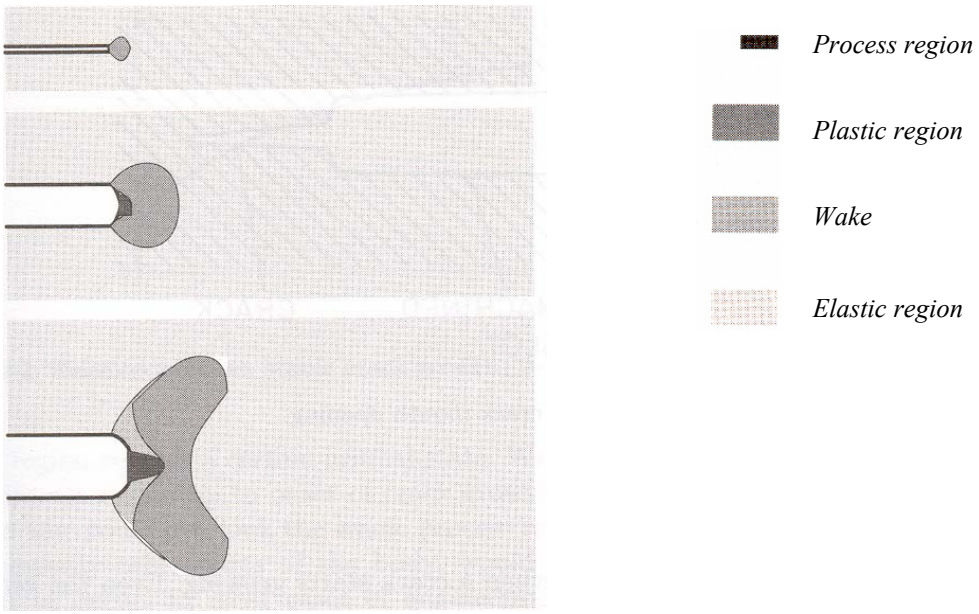

Figure 3.2 Blunting caused by plastic flow near the crack edge during loading of an originally sharp crack - Stretched zone

The sequence of events is illustrated in Figure 3.2. During loading without crack growth, the plastic flow near the crack edge and the height increase of the process region causes considerable *blunting* of the edge, forming the so-called *stretched zone.* In some materials, for instance mild steel, the blunting may be visible by the naked eye. A machine produced pre-existing crack may be substantially blunted; this may lead to considerably increased resistance to onset of crack growth.

Blunting may be studied experimentally in different ways. It can be observed optically in a cut normal to the crack edge. Another way is to pour a mould into the crack, which is withdrawn after the mould has solidified and the crack has been opened. In a less direct way, a CMOD-measurement (Crack Mouth Opening Displacement), the change in crack opening during loading is determined at the crack mouth, generally by means of a clip-gauge (Figure 3.3). This method, which is extensively used in fracture mechanics tests, is known as CTOD-determination (Crack Tip Opening Displacement). It is based on some estimated relation between crack blunting and mouth opening, assuming that the crack has not grown.

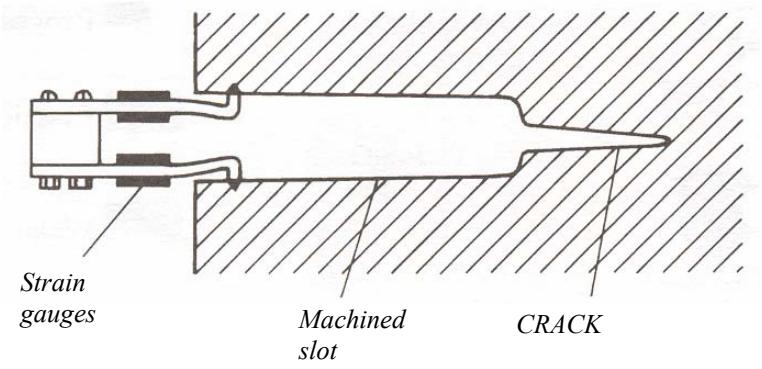

Figure 3.3 Clip-gauge measurement of crack mouth opening

3.4 Onset of Crack Growth

It is usually very difficult to detect when a crack starts growing. Even the very concept of incipient crack growth is difficult to define. Crack growth occurs when micro separations in front of the crack edge coalesce with the main crack, but the

micro separations are, unevenly spaced and of different sizes. They may even be of different types along the crack edge. Some coalescence with the main crack may therefore occur long before coalescences along the major part of the edge. Even from a macroscopic point of view, crack growth may occur early along some part of the crack edge and later at other parts, as at the "thumbnail effect".

The difficulty in identifying incipient crack growth is similar to that encountered in the determination of the "elastic limit" from a tensile test. In that case the difficulty is resolved by a convention, the idea of which is to define the yield stress as the stress when a small, but Jet safely detectable permanent elongation (usually 0.2%) has occurred. The same idea, applied to crack growth, leads to definition of incipient crack growth as the state when a small, but yet safely detectable permanent of crack growth has occurred. Extraordinary and sophisticated techniques should not be needed. Methods to determine the amount of stable crack growth will be discussed in the next section.

A convention that allows unambiguous determination of incipient crack growth, like the one discussed, may be needed for testing purposes. In theoretical treatments, it is nevertheless usually assumed that onset of crack growth occurs smoothly and simultaneously along the whole crack edge. Such idealizations are common in applied mechanics: in elastic-plastic theories, for instance, the state is assumed to be completely elastic until the yield condition is reached, and homogeneous plastic flow is assumed to occur immediately afterwards.

The onset of crack growth depends on several factors: material properties, body geometry (including crack geometry), load distribution, load magnitude and environmental conditions. Time effects of ten play a part as a result of viscoplastic flow in the process region and its vicinity. In other cases diffusion of impurity atoms towards the process region may cause delayed onset of crack growth after lo ad application. Time effects will be more important the further the crack growth process proceeds toward 'unstable crack growth.

Onset of stable crack growth is governed by a *local condition,* describing when the process region reaches a certain critical state. With experience from the development of the process region up to onset of crack growth in a certain material, an imagined observer who could overlook the whole process region and its immediate vicinity, but not necessarily other parts of the body, would be able to tell when crack growth is about to occur. In most cases of engineering interest, the development of size, shape and deformations of the process region will always be the same in the same material: the observer will not be able to see any differences, except those related to the irregular distribution of micro-separations. This independence on body and loading geometry is what Barenblatt (1959) called *autonomy,* a concept that will be used frequently in the present work. It has played a dominating role in fracture mechanics, although of ten intuitively taken for granted rather than explicitly recognized. It should, however, be remarked already here that there are several exceptions to autonomy; thus, the loading situation (in particular whether it produces crack face opening or gliding) and environmental conditions have to be specified.

3.5 Basic Relations in Crack Mechanics

3.5.1 General Considerations

Because the process region cannot be treated as a continuum, crack and fracture problems cannot be solved simply by calculating stresses and strains in the body. On the other hand, knowledge of stresses and strains in the continuum outside the process region is essential for understanding the process of crack growth and fracture. Both analytical and numerical calculations play important roles. Analytical methods are generally based on partial differential equations or integral equations. Among numerical methods the finite element methods dominate.

Due to the complexity of real phenomena concerning cracks and fracture, analytical methods almost invariably require highly idealized models of body geometry, process region characteristics and continuum constitutive equations.

Nevertheless, analytical solutions give an insight into and an understanding about basic relations that might be difficult to identify and extract from numerical treatments. Analytical solutions, particularly exact ones, are also very useful for controlling the accuracy of numerical methods, or even to test such methods for possible errors.

3.5.2 Boundary Conditions

Most crack problems are boundary value problems. Conditions on boundaries of the continua may be divided into the following three categories:

1. Conditions on the outer boundaries of the body, including the crack faces. These conditions usually consist of specification of tractions and/or displacements.

2. Continuity conditions on the interfaces between different regions in the continuum, such as the elastic region, the plastic region and its wake or regions occupied by different materials. These conditions are automatically taken care of in some treatments, for instance finite element calculations.

3. Conditions on the boundary to the process region. These conditions depend on the response of the process region model to loads or displacements.

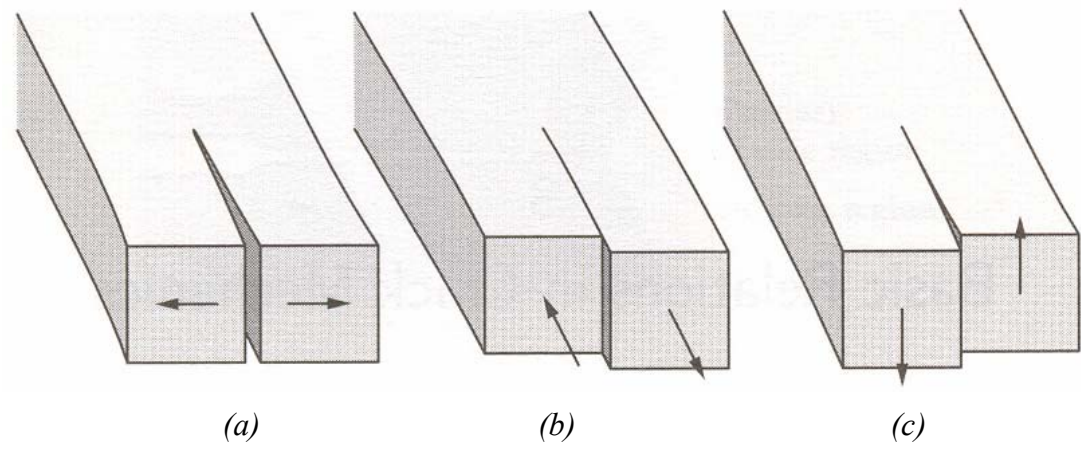

Figure 3.4 Symmetry modes, a) The in-plane opening mode, b) The in-plane shearing mode, c) The anti-plane shearing mode

3.5.3 The Three Symmetry Modes

In order to avoid complications, general discussions in the following will, unless otherwise stated, refer to eases in which the stress-strain field near the crack edge possesses certain symmetry properties. For linear problems, this does not impose a limitation, because each such problem may be considered as a superposition of three part-problems, each possessing symmetry properties near the crack edge, so-called symmetry *modes.* These modes were introduced by Irwin (1960), and they play an enormously important part in structuring the analysis of cracks and fracture. They are

1 – *The opening mode,* explained by Figure 3.4.a. This mode is traditionally referred to as mode I. Two varieties, plane strain and plane stress, are of special interest.

2 – *The in-plan e shearing* (or gliding) mode, explained by Fig. 3.4.b. This mode is traditionally referred to as mode II. Also for this mo de the two varieties, plane strain and plane stress, are of special interest.

3 – *The anti-plane shearing* (or gliding) mode, explained by Fig. 3.4.c. This mode is traditionally referred to as mo de III.

The terms *"in-plane"* and *"anti-plane"* do not imply that only plane problems are considered. The crack edge does not necessarily need to be straight. A penny-shaped (circular) crack in a large body may be loaded in the opening mode around its whole periphery or it may be loaded in mixtures of the two shearing modes. If it is subjected to arbitrary loading, it is possible to make a division into the three modes for any sufficiently close vicinity of the crack edge along the periphery. This is also possible for a non-planar crack with arbitrary edge shape.

With a coordinate system as shown in Figure 3.5, and with *u, v, w* being the components of the displacement vector *u,* the three mo des may be specified as follows ("horizontal" refers to the *x* direction, "vertical" to the *y* direction):

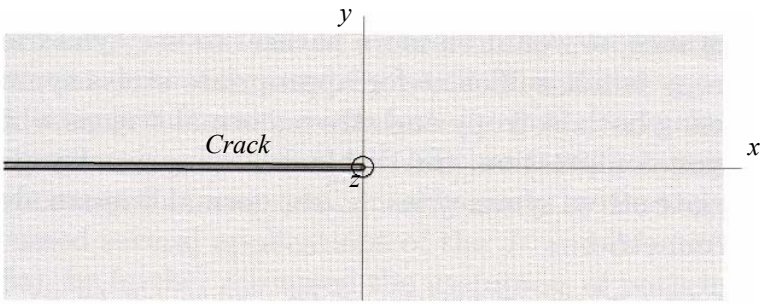

Figure 3.5 Crack edge neighborhood and coordinate system

Mode I. Horizontal displacements are symmetric, vertical displacements anti-symmetric:

$$u(x,-y,z)=u(x,y,z)\,, \qquad v(x,-y,z)=-v(x,y,z) \tag{3.1}$$

$$w=0 \quad (plane\ strain)\ , \qquad \frac{\partial^2 w}{\partial z^2}=0\ \ (plane\ \ stress) \tag{3.2}$$

Mode II. Horizontal displacements are anti-symmetric, vertical displacements symmetric:

$$u(x,-y,z)=-u(x,y,z)\,, \qquad v(x,-y,z)=v(x,y,z) \tag{3.3}$$

$$w=0 \quad (plane\ strain)\ , \qquad \frac{\partial^2 w}{\partial z^2}=0\ \ (plane\ \ stress) \tag{3.4}$$

Mode III. The only non-vanishing displacement, w is anti-symmetric:

$$u=v=0 \qquad w(x,-y,z)=-w(x,y,z)\ , \qquad \frac{\partial w}{\partial z}=0 \tag{3.5}$$

It is also required that the three modes possess certain stress symmetries. These are automatically satisfied for modes I and III if the displacement symmetries are

satisfied and the material is isotropic. Thus:

Mode I. Normal stresses are symmetric, shear stresses anti-symmetric:

$$\sigma_x(x,-y,z)=\sigma_x(x,y,z), \qquad \sigma_y(x,-y,z)=\sigma_y(x,y,z) \tag{3.6}$$

$$\sigma_z(x,-y,z)=\sigma_z(x,y,z), \qquad \tau_{xy}(x,-y,z)=-\tau_{xy}(x,y,z) \tag{3.7}$$

$$\tau_{xz}=\tau_{yz}=0 \tag{3.8}$$

Mode III. The only non-vanishing stresses are τ_{xz}, anti-symmetric, and, τ_{yz} symmetric:

$$\sigma_x=\sigma_y=\sigma_z=\tau_{xy}=0 \tag{3.9}$$

$$\tau_{xz}(x,-y,z)=-\tau_{xz}(x,y,z), \quad \tau_{yz}(x,-y,z)=\tau_{xy}(x,y,z) \tag{3.10}$$

$$\frac{\partial\tau_{xz}}{\partial z}=\frac{\partial\tau_{yz}}{\partial z}=0 \tag{3.11}$$

For in-plane problems, there is no dependence on the anti-plane coordinate z, except for *w* in mode II. Thus, $u=u(x,y)$, $\sigma_y=\sigma_y(x,y)$, etc. For non-plane problems, curvilinear rather than Cartesian coordinates may be more convenient. For the penny-shaped crack, for instance, it would be more natural to use cylindrical coordinates.

For mode II, isotropy is not sufficient for appropriate stress symmetries. However, for a material possessing both isotropy and stress-strain relations which are symmetric with respect to tension-compression, the displacement symmetry properties of mo de II imply the appropriate stress symmetries. Then, normal stresses are anti-symmetric and shear stresses are symmetric:

$$\sigma_x(x,-y)=-\sigma_x(x,y), \qquad \sigma_y(x,-y)=-\sigma_y(x,y) \tag{3.12}$$

$$\sigma_z(x,-y)=-\sigma_z(x,y), \qquad \tau_{xy}(x,-y)=\tau_{xy}(x,y) \tag{3.13}$$

$$\tau_{xz} = \tau_{yz} = 0 \tag{3.14}$$

However, few, if any, stress-strain relations are symmetric with respect to tension compression in non-linear regions. Therefore, pure mode II conditions are hardly possible to realize exactly in the continuum close to the process region, but in practical situations, such as earthquake sliding motion, they may still be assumed to prevail with sufficient accuracy.

Isotropy is not an absolute condition for symmetry mode relations; certain kinds of anisotropy may be allowed, if the crack is properly oriented with respect to the anisotropy directions. Similarly, separate treatment of the three modes is very fruitful for non-linear cases, even though the convenient principle of superposition does not hold. In this context, it should be noted that many practical situations involve pure modes, so the need for superposition of modes is generally not a problem.

In some linear cases, it is impossible to make a partition into symmetry modes. One example of considerable practical interest is the interface crack, for which the displacement pattern in the crack edge vicinity is incompatible with such a partition.

3.6 Path-independent Integrals

3.6.1 General Considerations

For elastic stress-strain fields, a surface-integral representation of a property related to the presence of a defect (a singularity or an inhomogeneity) was derived by Eshelby (1957), based on an earlier work (Eshelby 1951). He noticed that the integral vanished for a closed surface, embracing a homogeneous elastic material, even with allowance for anisotropy and finite deformation. Later, Günther (1962), obviously unaware of Eshelby' s results, introduced some similar surface- and line-integrals, also with conservation properties, i.e. vanishing for closed surfaces or paths. Cherepanov (1967) and Rice (1968) introduced a path-independent integral, the J-integral, for plane elastostatic fields. It was later identified as a special ease of the

integral established by Eshelby, but it was mainly due to the paper by Rice (1968) that its potential as a tool for analysis of cracks was recognized. It has been extensively applied in fracture mechanics, especially in formulations of crack growth criteria.

The path-independent integral introduced by Cherepanov (1967) was derived for a moving crack. It also took heat flow, body forces and inertia into consideration, but the path was assumed to be drawn sufficiently close the crack edge to avail of asymptotic properties in this vicinity.

3.6.2 A Path-independent Integral for Plates

An extension of the *J*-integral to a path-integral for a plate subjected to in-plane loading was given by Broberg (1979, 1987). This integral may be written

$$P = \int_{\Gamma} \left[W_{av} dx_2 - \left(n_j \sigma_{ji} \partial u_i / \partial x_1 \right)_{av} ds \right] \qquad (i = 1,\ 2,3\ ;\ j = 1,\ 2) \tag{3.15}$$

where subscript *av* indicates the average over the plate thickness, Γ is a path in the mid-plane of the plate, W the stress-strain energy per unit volume, n_j a unit normal to Γ, u_i the displacement, x_j Cartesian coordinates with x_3 in the thickness direction, right, seen from the positive x_3 side (Figure 3.6).

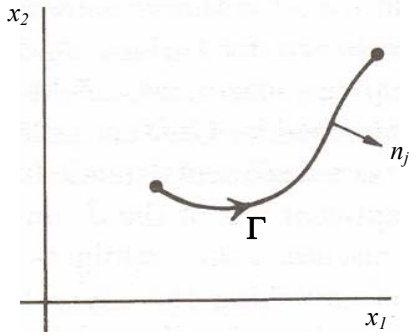

Figure 3.6 Plate integral

The stress σ_{ij} (i, j=1, 2, 3) is defined by the relation

$$\sigma_{ji} = \frac{\partial W}{\partial u_{i,j}} \quad \text{(i, j=1, 2, 3)} \tag{3.16}$$

where

$$u_{i,j} = \frac{\partial u_i}{\partial x_j} \tag{3.17}$$

The stress tensor σ_{ij} as defined by equation (3.16), which is not restricted to small deformations, is not, symmetric, except for $\left|u_{i,j}\right| << 1$, but the equilibrium equations take the simple form

$$\sigma_{ji,j} = 0 \tag{3.18}$$

where the summation convention is used.

3.7 Fracture Toughness Testing

A fracture toughness test measures the resistance of a material to crack extension. Such a test may yield cither a single value of fracture toughness or a resistance curve, where a toughness parameter such as *K, J,* or *CTOD* is plotted against crack extension. A single toughness value is usually sufficient to describe a test that fails by cleavage, because this fracture mechanism is typically unstable. Cleavage fracture actually has a falling resistance curve. Crack growth by microvoid coalescence, however, usually yields arising *R* curve; ductile crack growth can be stable, at least initially. When ductile crack growth initiates in a test specimen, that specimen seldom fails immediately. Therefore, one can quantify ductile fracture resistance either by the initiation value or by the entire *R* curve.

A variety of organizations throughout the world publish standardized procedures for fracture toughness measurements, including the American Society for Testing and Materials (ASTM), the British Standards Institution (BSI), the International Institute of Standards (ISO) and the Japan Society of Mechanical Engineers (JSME). The first standards for *K* and *J* testing were developed by ASTM in 1970 and 1981, respectively, while BSI published the first *CTOD* test method in 1979.

3.7.1 General Considerations

Virtually all fracture toughness tests have several common features. The design of test specimens is similar in each of the standards and the orientation of the specimen relative to symmetry directions in the material is always an important consideration. The cracks in test specimens are introduced by fatigue in each case, although the requirement for fatigue loads varies from one standard to the next. The basic instrumentation required measuring load and displacement is common to virtually all fracture mechanics tests, but some tests require additional instrumentation to monitor crack growth.

3.7.2 Specimen Configurations

There are five types of specimens that are permitted in ASTM standards that characterize fracture initiation and crack growth, although no single standard allows all five configurations, and the design of a particular specimen type may vary between standards. The configurations that are currently standardized include the compact specimen, the single edge notched bend (SENB) geometry, the arc-shaped specimen, the disk specimen, and the middle tension (MT) panel. Figure 3.7 shows a drawing of each specimen type.

Each specimen configuration has three important characteristic dimensions: the crack length (a), the thickness (B) and the width *(W)*. In most cases, $W = 2B$ and $a/W \approx 0.5$.

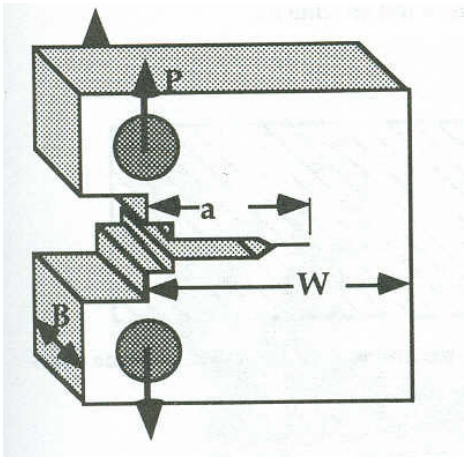

(a) Compact specimen

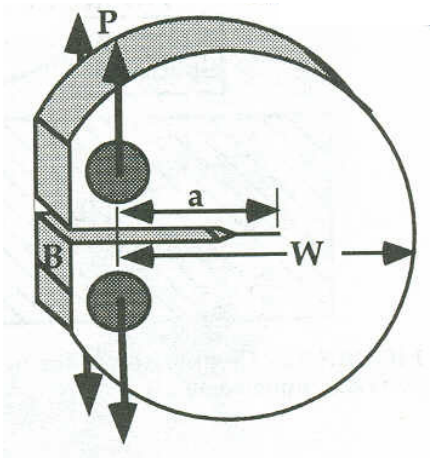

(b) Disk shaped compact specimen

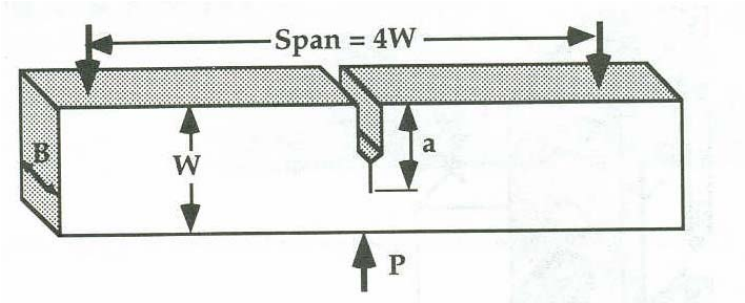

(c) Single edge notched bend (SENB) specimen

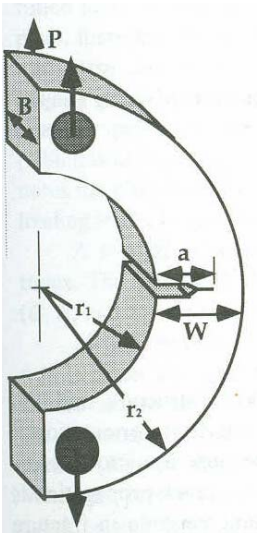

(d) Arc shaped specimen

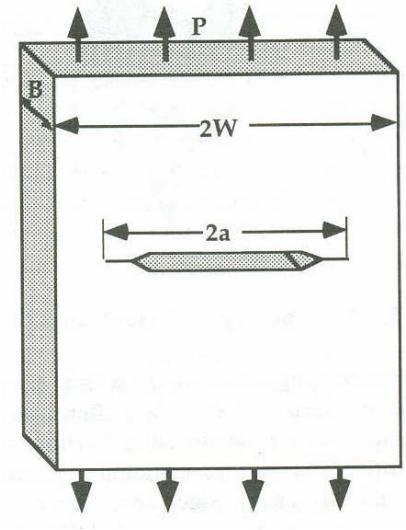

(e) Middle tension (MT) specimen

Figure 3.7 Specimen types

There are number of specimen configurations that are used in research, but have yet to be standardized. Some of the more common nonstandard configurations include the single edge notch tensile panel, the double edge notched tensile panel, the axisymmetric notched bar, and the double cantilever beam specimen.

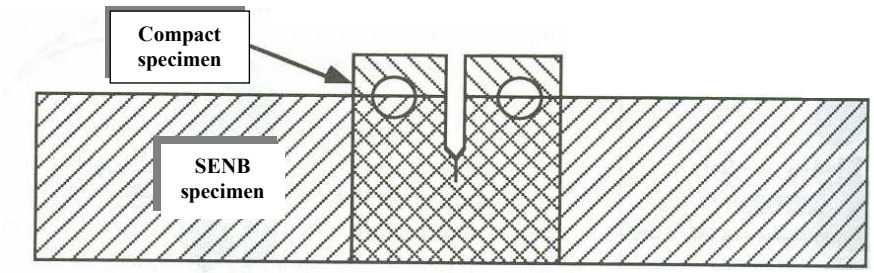

Figure 3.8 Comparison of the profiles of compact and SENB specimens with the same-in-plane characteristic dimensions

The vast majority of fracture toughness tests are performed on either compact or SENB specimens. Figure 3.8 illustrates the profiles of these two specimen types, assuming the same characteristic dimensions *(B, W, a)*. The compact geometry obviously consumes less material, but this specimen requires extra material in the width direction, due to the holes. If one is testing plate material or a forging, the compact specimen is more economical, but the SENB configuration may be preferable for weldment testing, because less weld metal is consumed in some orientations.

The compact specimen is pin-loaded by special clevises, as illustrated in Fig. 3.9. Compact specimens are usually machined in a limited number of sizes, because a separate test fixture must be fabricated for each specimen size. Specimen size is usually scaled geometrically; standard sizes include: 1/2T, 1T, 2T and 4T, where the nomenclature refers to the thickness in inches 1. For example, a standard IT compact specimen has the dimensions $B = 1$ in (25.4 mm) and $W = 2$ in (50.8 mm). Although ASTM has converted to SI units, the above nomenclature for compact specimen sizes persists.

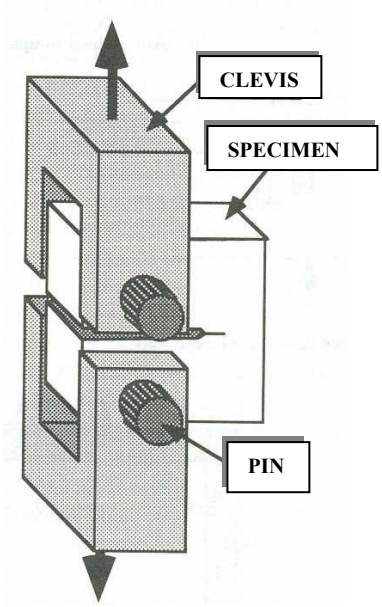

Figure 3.9 Apparatus for testing compact specimen

The SENB specimen is more flexible with respect to size. The standard loading span for SENB specimens is *4W*. If the fixture is designed properly, the span can be adjusted continuously to any value that is within its capacity. Thus SENB specimens with a wide range of thicknesses can be tested with a single fixture.

3.7.3 K_{Ic} Testing

When a material behaves in a linear elastic manner prior to failure, such the plastic zone is small compared to specimen dimensions, a critical value of the stress intensity factor, K_{Ic}, may be an appropriate fracture parameter. Standard methods for K_{Ic} testing include ASTM E 399 and BS 5447, the latter of which was published by the British Standards Institution.

The ASTM standard E 399 was first published in 1970, and has been revised several times since then. The title, *"Standard Test Method for Plane Strain Fracture Toughness* of *Metallic Materials"* is somewhat misleading. Although plane strain is a necessary condition for a valid K_{Ic} test, it is not sufficient; a specimen must also behave in a linear elastic manner.

Four specimen configurations are permitted by the current version of E 399: the compact, SENB, arc-shaped, and disk-shaped specimens. Specimens for K_{Ic} tests are usually fabricated with the width, W, equal to twice the thickness, B. They are fatigue precracked so that the crack length/width ratio (a/W) lies between 0.45 and 0.55. Thus the specimen design is such that all the critical dimensions, a, B, and $W-a$, are approximately equal. This design results in efficient use of material, since each of these dimensions must be large compared to the plastic zone.

Most standardized mechanical tests (fracture toughness and otherwise), lead to valid results as long as the technician follows all of the procedures outlined in the standard. The K_{Ic} test, however, often produces invalid results through no fault of the technician. If the plastic zone at fracture is too large, it is not possible to obtain a valid K_{Ic}, regardless of how skilled the technician is.

Because of the strict size requirements, ASTM E 399 recommends that the user perform a preliminary validity check to determine the appropriate specimen dimensions. The size requirements for a valid K_{Ic} are as follows:

$$B, a \geq 2.5\left(\frac{K_{Ic}}{\sigma_{YS}}\right)^2 \qquad 0.45 \leq a/W \leq 0.55 \tag{3.19}$$

In order to determine the required specimen dimensions, the user must make a rough estimate of the anticipated K_{Ic} for the material. Such an estimate can come from data for similar materials. If such data are not available, the ASTM standard provides a table of recommended thicknesses for various strength levels. Although there is a tendency for toughness to decrease with increasing strength, there is not a unique relationship between K_{Ic} and σ_{YS} in metals. Thus the strength-thickness table in E 399 should be used only when better data are not available.

During the initial stages of fatigue precracking, the peak value of stress intensity in a single cycle, K_{max}, should be no larger than $0.8K_{Ic}$, according to ASTM E 399.

As the crack approaches its final size, K_{max} should be less than $0.6K_{Ic}$. If the specimen is fatigued at one temperature (T_1) and tested at a different temperature (T_2), the final K_{max} must be $\leq 0.6[\sigma_{YS(1)}/\sigma_{YS(2)}]K_{Ic}$. The fatigue load requirements are less stringent at initiation because the final crack tip is remote from any damaged material that is produced in the early part of precracking. The maximum stress intensity during fatigue must always be less than *K/c,* however, in order to avoid premature failure of the specimen.

Of course, one must know *K/c* in order to determine the maximum allowable fatigue loads. The user must specify fatigue loads based on the anticipated toughness of the material. If he or she is conservative and selects low loads, precracking could take a very long time. On the other hand, if precracking is conducted at high loads, the user risks an invalid result, in which case the specimen and the technician's time are wasted.

When a precracked test specimen is loaded to failure, load and displacement are monitored. Three types of load-displacement curves are shown in Figure 3.10. The critical load, P_Q, is defined in one of several ways, depending on the type of curve. One must construct a 5% secant line (i.e. a line from the origin with a slope equal to 95% of the initial elastic loading slope) to determine P_5. In the case of *Type I* behavior, the load-displacement curve is smooth and it deviates slightly from linearity before ultimate failure at P_{max}. This nonlinearity can be caused by plasticity, subcritical crack growth, or both. For a *Type I* curve, $P_Q = P_5$. With a *Type II* curve, a small amount of unstable crack growth (i.e. a pop-in) occurs before the curve deviates from linearity by 5%. In this case P_Q is defined at the pop-in. A specimen that exhibits *Type III* behavior fails completely before achieving 5% nonlinearity. In such cases, $P_Q = P_{max}$.

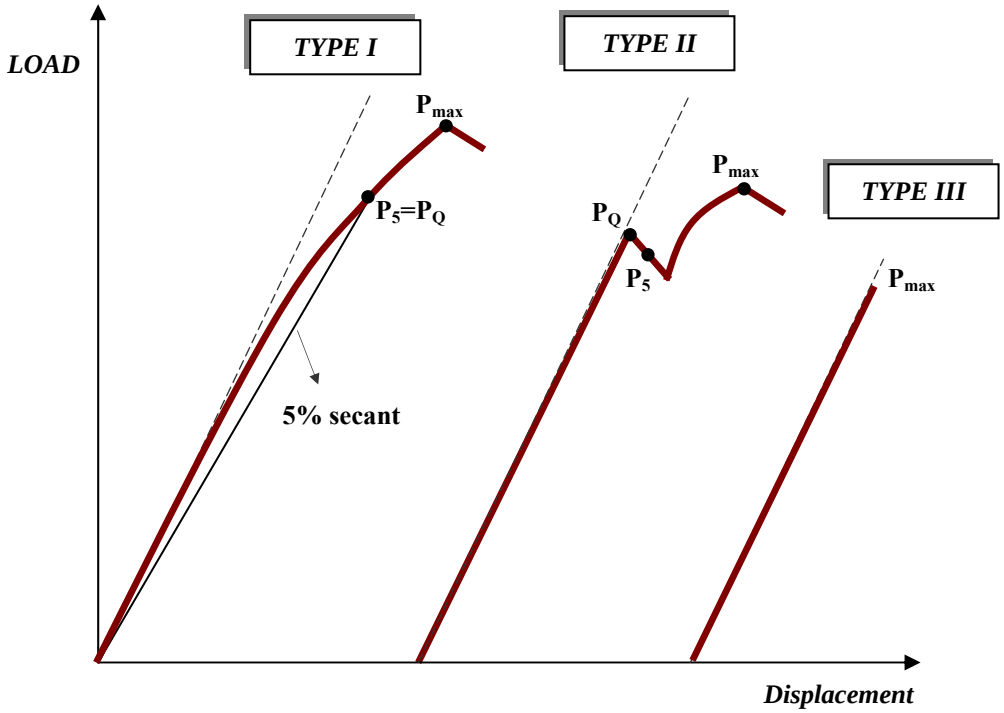

Figure 3.10 Three types of load-displacement behavior in a K_{Ic} test

The crack length must be measured from the fracture surface. Since there is a tendency for the crack depth to vary through the thickness, the crack length is defined as the average of three evenly spaced measurements. Once P_Q and crack length are determined, provisional fracture toughness, K_Q, is computed from the following relationship:

$$K_Q = \frac{P_Q}{B\sqrt{W}} f(a/W) \tag{3.20}$$

where *f(a/W)* is a dimensionless function of *a/W*. This function is given in polynomial form in the E 399 standard for the four specimen types. Individual values of *f(a/W)* are also tabulated in ASTM E 399.

The *KQ* value computed from Equation (3.20) is a valid K_{Ic} result only if all validity requirements in the standard are met, including

$$0.45 \le a/W \le 0.55 \tag{3.21a}$$

$$B, a \ge 2.5 \left(\frac{K_{Ic}}{\sigma_{YS}} \right)^2 \tag{3.21b}$$

$$P_{max} \le 1.10 P_Q \tag{3.21c}$$

Additional validity requirements include the restrictions on fatigue load mentioned earlier, as well as limits on fatigue crack curvature. If the test meets all of the requirements of ASTM E 399, then $K_Q = K_{Ic}$.

Recall that Equations (3.21a) and (3.21b) ensure that the critical specimen dimensions, *B, a,* and *(W–a),* are at least ~50 times larger than the plane strain plastic zone. The third requirement, Equation (7.3c), is necessary to correct a loophole in the K_{Ic} test procedure, as discussed below.

The deviation from linearity in a load-displacement curve can be caused by crack growth, plastic zone effects, or both. In the absence of plastic deformation, 5% deviation from the initial slope of the load-displacement curve corresponds to crack growth through approximately 2% of the ligament in test specimens with $a/W \approx 0.5$; when a plastic zone forms, a 5% deviation from linearity can be viewed as 2% apparent crack growth. If the nonlinearity in the load-displacement curve is caused only by plasticity, a 5% deviation from linearity corresponds to a plastic zone size that is roughly 2% (i.e. 1/50) of the uncracked ligament. *Thus the plastic zone size at PS in a Type I test is approximately equal to its maximum allowable size, as defined by Equation (3.21b).*

Consider a fracture toughness test that displays considerable plastic deformation prior to failure. Figure 3.11 schematically illustrates the load-displacement curve for such a test. Since this is a Type I *curve* $P_Q = P_5$. K_Q value computed from P_Q may just barely satisfy the size requirement of Equation (3.21b). Such a quantity, however, would have little relevance to the fracture toughness of the material, since the

specimen fails well beyond P_Q; the K_Q value in this case would grossly underestimate the true toughness of the material. Consequently the third validity requirement, Equation (3.21c), is necessary to ensure that a K_{Ic} value is indicative of true toughness of the material.

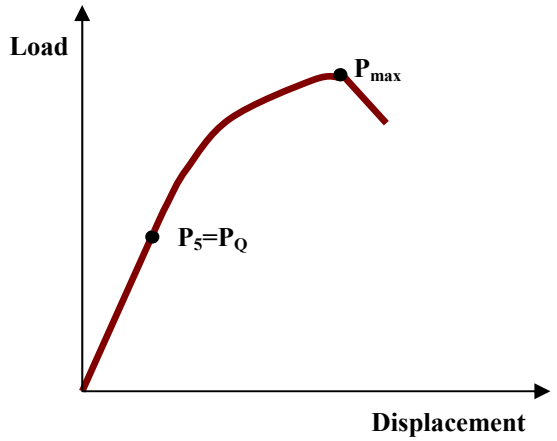

Figure 3.11 Load-displacement curve for an invalid K_{Ic} test, where ultimate failure occurs well beyond P_Q

Because the size requirements of ASTM E 399 are very stringent, it is very difficult and sometimes impossible to measure a valid K_{Ic} in most structural materials. A material must either be relatively brittle or the test specimen must be very large for linear elastic fracture mechanics to be valid. In low- and medium strength structural steels, valid K_{Ic} tests are normally possible only on the lower shelf of toughness; in the ductile-brittle transition and the upper shelf, elastic-plastic parameters such as the *J* integral and *CTOD* are required to characterize fracture.

Because of the strict validity requirements, the K_{Ic} test is of limited value to structural metals. The toughness and thickness of most materials precludes a valid K_{Ic} result. If, however, a valid K_{Ic} test can be measured on a given material, it is probably too brittle for most structural applications.

3.7.4 CTOD Testing

Because of the strict limits on plastic deformation, the K_{Ic} test can be applied only on the lower shelf of toughness in structural steels and welds. The older ASTM J_{Ic} and *J–R* curve test methods allow considerably more plastic deformation, but these tests are only valid on the upper shelf. Until the newer standards are published, the *CTOD* test is the only standardized method to measure fracture toughness in the ductile-brittle transition region.

The first *CTOD* test standard was published in Great Britain in 1979. ASTM recently published E 1290, an American version of the *CTOD* standard. The British *CTOD* standard allows only the SENB specimen, while the ASTM standard provides for *CTOD* measurements on both the compact and SENB specimens. Both standards allow two configurations of SENB specimens: 1) a rectangular cross section with *W=2B,* the standard geometry for K_{Ic} and J_{Ic} tests; and 2) a square cross section with *W =B*.

Experimental *CTOD* estimates are made by separating the *CTOD* into elastic and plastic components, similar to the J_{Ic} and *J–R* tests. The elastic *CTOD* is obtained from the elastic *K:*

$$\delta_{el} = \frac{K^2\left(1-\upsilon^2\right)}{2\sigma_{YS}E} \tag{3.22}$$

The elastic *K* is related to applied load through Equation (3.20). The above relationship assumes that d_n=0.5 for linear elastic conditions. The plastic component of *CTOD* is obtained by assuming that the test specimen rotates about a plastic hinge. This concept is illustrated in Figure 3.12 for an SENB specimen. The plastic displacement at the crack mouth, V_p, is related to the plastic *CTOD* through a similar triangles construction:

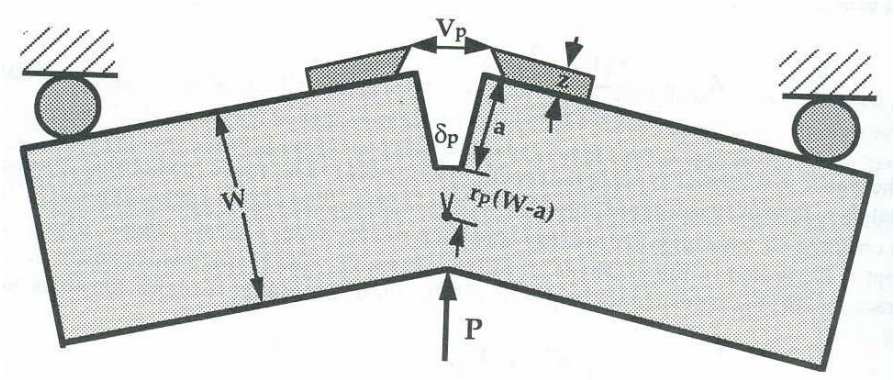

Figure 3.12 Hinge model for plastic displacements in an SENB specimen

$$\delta_{pl} = \frac{r_p(W-a)V_p}{r_p(W-a)+a+z} \tag{3.23}$$

where r_p is the plastic rotational factor, a constant between 0 and 1 that defines the relative position of the apparent hinge point. The mouth opening displacement is measured with a clip gage. In the cage of an SENB specimen, knife edges must often be attached in order to hold the clip gage. Thus Equation (3.23) must take account of the knife edge height, z. The compact specimen can be designed so that z=0. The plastic component of V is obtained from the load-displacement curve by constructing a line parallel to the elastic loading line. According to ASTM E 1290, the plastic rotational factor is given by

$$r_p=0.44 \tag{3.24a}$$

for the SENB specimen and

$$r_p = 0.4\left\{1+2\left[\left(\frac{a_o}{b_o}\right)^2+\frac{a_o}{b_o}+0.5\right]^{1/2}-2\left[\frac{a_o}{b_o}+0.5\right]\right\} \tag{3.24b}$$

for the compact specimen. The original British standard for CTOD tests, BS

5762:1979 applied only to SENB specimens and specified $r_p = 0.40$.

The crack mouth opening displacement, V, on an SENB specimen is not the same as the load line displacement, Δ. The *CTOD* standard utilizes V_p because this displacement is easier to measure in SENB specimens. If r_p is known, however, it is possible to infer J from a P- V curve or *CTOD* from a $P–\Delta$ curve. The compact specimen simplifies matters somewhat because $V = \Delta$ as long as $z = 0$.

The British ASTM *CTOD* standard test methods can be applied to ductile and brittle materials, as well as steels in the ductile-brittle transition. These standards include a notation for critical *CTOD* values that describes the fracture behavior of the specimen:

δ_e – Critical *CTOD* at the onset of unstable fracture with less than 0.2 mm of stable crack growth. This corresponds to the lower shelf and tower transition region of steels where the fracture mechanism is pure cleavage.

δ_u – Critical CTOD at the onset of unstable fracture which has been preceded by more than 0.2 mm of stable crack growth. In the case of ferritic steels, this corresponds to the "ductile thumbnail" observed in the upper transition region.

δ_i – *CTOD* near the initiation of stable crack growth. This measure of toughness is analogous to J_{Ic}.

δ_m – *CTOD* at the first attainment of a maximum load plateau. This occurs on or near the upper shelf of steels.

Figure 3.13 is a series of schematic load-displacement curves that manifest each of the above failure scenarios. Curve (a) illustrates a test that results in a δ_c value; cleavage fracture occurs at P_i. Figure 3.13.b corresponds to a δ_u result, where ductile tearing precedes cleavage. The ductile crack growth initiates at P_j. A test on or near the upper shelf produces a load-displacement curve like Figure 3.13.c; a maximum

load plateau occurs at P_m. The specimen is still stable after maximum load because the material has arising R curve and the test is performed in displacement control. Three types of *CTOD* result, δ_c, δ_u and δ_m, are mutually exclusive; i.e., they cannot occur in the same test. It is possible, however, to measure a δ_i value in the same test as either a δ_m or δ_u result.

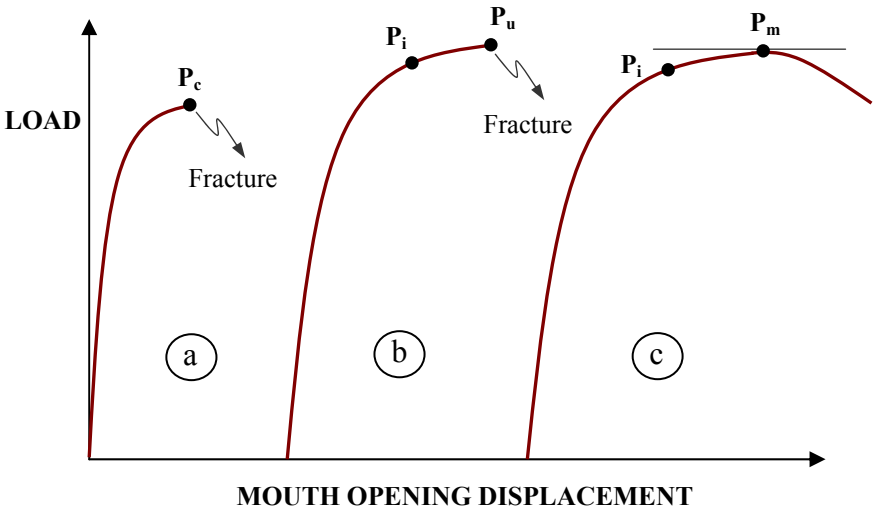

Figure 3.13 Various types of load-displacement curves from CTOD tests

As Figure 3.13 illustrates, there is usually no detectable change in the load-displacement curve at P_i. The only deviation in the load-displacement behavior is the reduced rate of increase in load as the crack grows. The maximum load plateau (Figure 3.13.c) occurs when the rate of strain hardening is exactly balanced by the rate of decrease in the cross section. However, the initiation of crack growth cannot be detected from the load-displacement curve because the loss of cross section is gradual. Thus δ_i must be determined from an R curve.

The only specimen size requirement of the British and ASTM *CTOD* standards is a recommendation to test full section thicknesses. For example, if a structure is to be made of 25 mm (1 in) thick plate, then B in the test specimens should be nominally 25 mm. if the specimen is notched from the surface, a square section specimen is required for B to equal the plate thickness. The British *CTOD* standard allows a/W

ratios ranging from 0.15 to 0.70, while the ASTM standard restricts the permissible *a/W* values to the range of 0.45 to 0.55. Shallow cracked specimens have certain advantages, particularly for weldment tests, but critical *CTOD* values from such tests are usually geometry dependent.

CHAPTER FOUR
ELASTO-PLASTIC FINITE ELEMENT ANALYSIS

4.1 Introduction

In structural mechanics, a problem is nonlinear if the stiffness matrix or the load vector depends on the displacements. Nonlinearity in structures can be classed as *material nonlinearity* (associated with changes in material properties, as in plasticity) or as *geometric nonlinearity* (associated with changes in configuration, as in large deflections of a slender elastic beam). In general, for a time-independent problem symbolized as

$$[\mathbf{K}]\{\mathbf{D}\} = \{\mathbf{R}\} \tag{4.1}$$

in *linear* analysis both [**K**] and {**R**} are regarded as independent of {**D**}, whereas in *nonlinear* analysis [**K**] and/or {**R**} are regarded as {**D**}.

The classifications “linear” and “nonlinear” are artificial in that physical reality presents various problems, some of which can be satisfactorily approximated by linear equations. Nonlinear approximations are more difficult to formulate, and solving the resulting equations may cost 10 or 100 times as much as linear approximation having the same number of degrees of freedom.

Many physical situations present nonlinearities too large to be ignored. Stress-strain relations may be nonlinear in either in a time-dependent or a time-independent way. A change in configuration may cause loads to alter their distribution and magnitude or cause gaps to open or close. Mating parts may stick or slip. Welding or casting processes cause the material to change in conductivity, modulus or phase.

4.2 Solution Methods

A representative time-independent nonlinear problem can be stated as Equation (4.1), where {**R**} is known and [**K**] is a function of {**D**} that can be computed for a given {**D**}.{**D**} is required to compute –for example the displacement state associated with known loads.

Consider a nonlinear spring, Figure 4.1, the source of the nonlinearity is unimportant. If the spring stiffness k is composed of a constant, term k_o and a term k_N that depends on deformation, displacement u is caused by load P and is given by the equation

$$(k_o + k_N)u = P \qquad where \;\; k_N = f(u) \tag{4.2}$$

4.2.1 Direct Substitution

Let a load P_A be applied to a softening spring (for which $k_N < 0$). For the first iteration, it is assumed that k_N=0. Therefore, as the first approximation of displacement u_A produced by P_A, u_1 is computed as $u_1=P_A/k_o$. Using u_1, the new stiffness approximation

$$k_o + k_{N1} = k_o + f(u_1) \tag{4.3}$$

and then, the new displacement approximation u_2.

Thus general the sequence of approximations

$$u_1 = k_o^{-1} P_A \;,\; u_2 = (k_o + k_{N1})^{-1} P_A \;, \ldots\ldots, u_{i+1} = (k_o + k_{Ni})^{-1} P_A \tag{4.4}$$

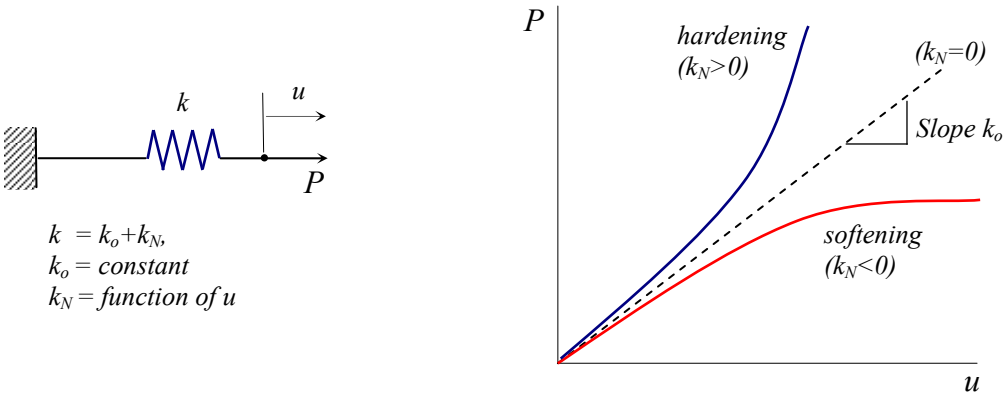

Figure 4.1 A nonlinear spring and its load-displacement curve

These calculations are interpreted graphically in Figure 4.1. As seen from the figure, the approximate stiffnesses k_o+k_{Ni} can be regarded as secants of the actual curve, each emanating from $P=u=0$. After several iterations, the secant stiffness is $k_o+k_N \approx P_A/u_A$, and the correct solution $u=u_A$ is closely approximated.

In an alternative form of direct substitution, nonlinear terms $k_N u$ are taken to the rigth-hand side. Thus, instead of equation (4.4), the sequence

$$u_1 = k_o^{-1} P_A \ , \ u_2 = k_o^{-1}\left(P_A - k_{N1}u_1\right), \ldots\ldots, u_{i+1} = k_o^{-1}\left(P_A - k_{Ni}u_i\right) \tag{4.5}$$

(Equations (4.4) and (4.5) will not yield the same values of u_2, u_3, etc., but upon convergence both will yield the result $u_\infty=u_A$). Equation (4.5) is interpreted graphically in Figure 4.2-b. the effective loads applied in the second and third iterations in Figure 4.2-b are

$$P_A - k_{N1}u_1 = P_A + \left[k_o u_1 - \left(ko + k_{N1}\right)u_1\right] = P_A + \left(P_a - P_1\right) \tag{4.6}$$

$$P_A - k_{N2}u_2 = P_A + \left[k_o u_2 - \left(ko + k_{N2}\right)u_2\right] = P_A + \left(P_1 - P_2\right) \tag{4.7}$$

It may be helpful to note that $P_a - P_1 = P_1 - P_A$ and $P_1 - P_2 = P_{II} - P_A$. The sequence of pseudo loads $P_a - P_1$, $P_1 - P_2$,...., must converge if Equation (4.5) is converge to $u = u_A$. Failure to converge is more likely with hardening structures than with softening structures.

If convergence difficulties arise, under relaxation may help. Thus, rather than updating a calculated value u_{i+1} to its full value, updating instead to

$$u_{i+1} = u_i + \beta(\Delta u_{i+1}) \tag{4.8}$$

or, changing the form by the substitution $\Delta u_{i+1} = u_{i+1} - u_i$,

$$u_{i+1} = \beta u_{i+1} + (1-\beta)u_i \tag{4.9}$$

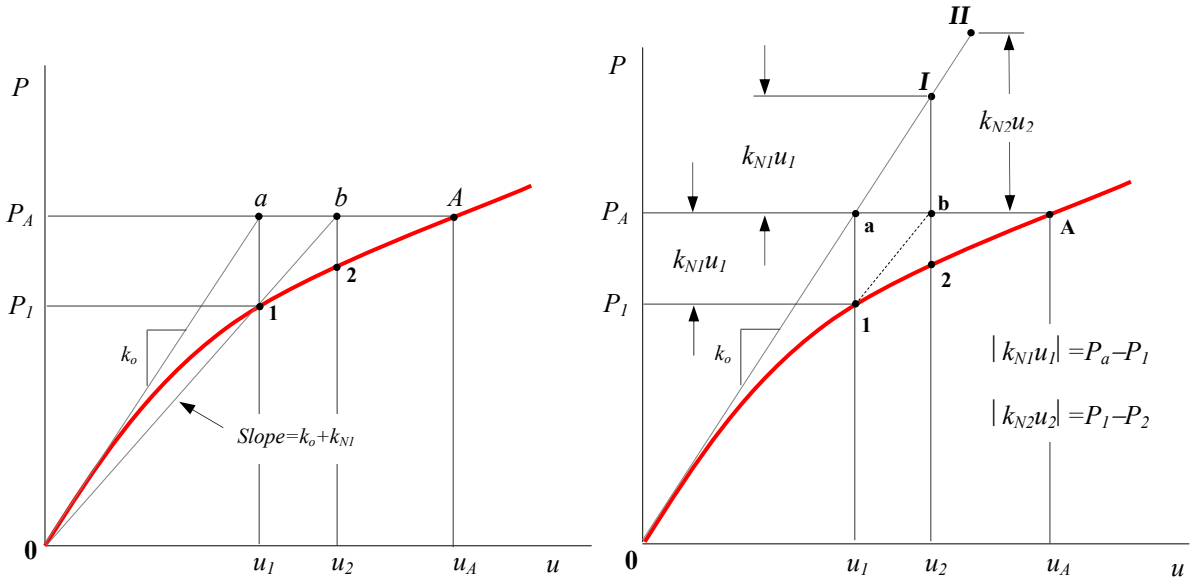

Figure 4.2 Graphical interpretations of direct substitution

4.2.2 Newton-Raphson (N-R)

Consider that P_A is the applied load and somehow determined the corresponding displacement u_A. That is, from Equation (4.2),

$$\left(k_o + k_{NA}\right)u_A = P_A \qquad where \;\; k_{NA} = f(u_A) \tag{4.10}$$

The load is increased to value P_B and the corresponding displacement u_B is sought. A truncated Taylor series expansion of $P=f(u)$ about u_A is

$$f\left(u_A + u_1\right) = f\left(u_A\right) + \left(\frac{dP}{du}\right)_A \Delta u_1 \tag{4.11}$$

where

$$\frac{dP}{du} = \frac{d}{du}\left(k_o u + k_N u\right) = k_o + \frac{d}{du}\left(k_o u + k_N u\right) = k_t \tag{4.12}$$

and k_t is called the *tangent stiffness*. Δu_1 is determined for which $f(u_A+\Delta u_1)=P_B$. Thus, with $f(u_A)=P_A$ and k_t evaluated at A, Equation (4.11) becomes

$$P_B = P_A + \left(k_t\right)_A \Delta u_1 \qquad or \qquad \left(k_t\right)_A \Delta u_1 = P_B - P_A \tag{4.13}$$

where $P_B–P_A$ can be interpreted as a load imbalance, as the difference between the applied load P_B and the force $P_A = \left(k_o + k_{NA}\right)u_A$ in the spring when its stretch is u_A. The solution process is depicted in Figure 4.4-a. After computing Δu_1, update the displacement estimate to $u_1=u_A+\Delta u_1$. For the next iteration, new tangent stiffness $(k_t)_1$ is obtained by use of Equation (4.12) with $u=u_1$, and new load imbalance $P_B–P_1$, where P_1 comes from Equation (4.2) with $u=u_1$. The updated displacement estimate is $u_2=u_1+\Delta u_2$, where Δu_2 is obtained by solving $(k_t)_1\Delta u_2=P_B–P_1$.

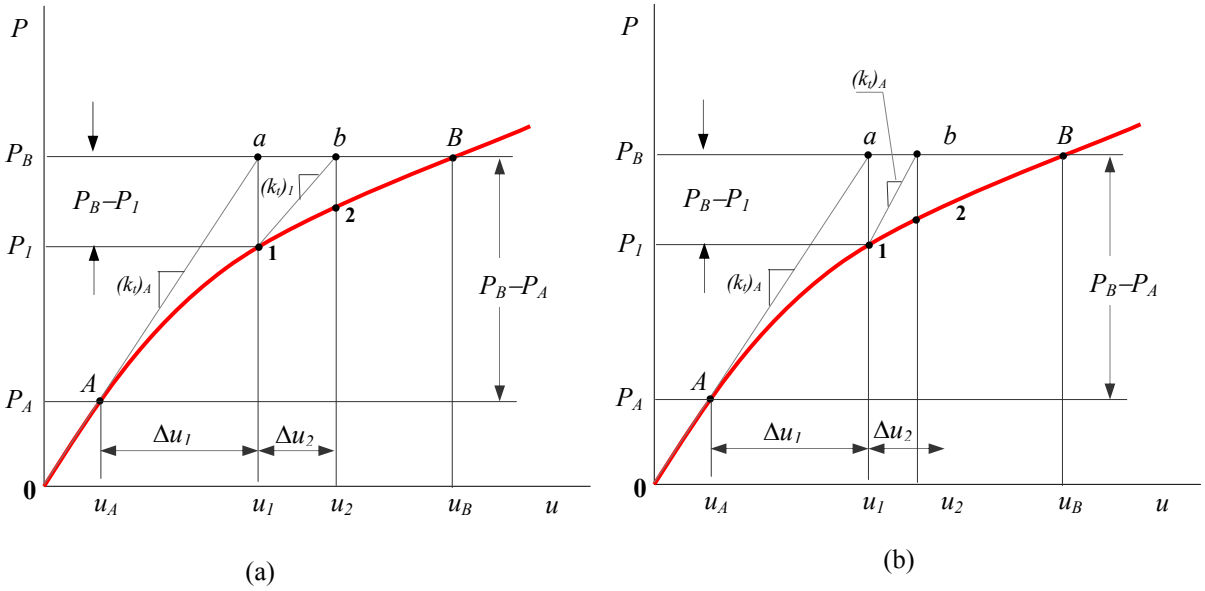

Figure 4.3 a) N–R solution b) Modified N–R solution

4.2.3 Modified Newton-Raphson

This method differs from the N-R method only in that the tangent stiffness either is not updated or is updated infrequently. Thus, in multi d.o.f. problems, it is important to avoid the expensive repetitions of forming and reducing the tangent-stiffness $[K_t]$. However, more iterative cycles are needed in order to reach a prescribed accuracy. The process is depicted one-dimensional in Figure 4.3-b.

If $[K_t]$ is referred to the initial configuration, the modified N-R method becomes almost identical to direct substitution method of Equation (4.4). The only difference is that modified N-R computes u_{i+1} by adding u_{i+1} to u_i, and Equation (4.4) computes u_{i+1} directly.

CHAPTER FIVE
MODEL DESIGN IN ABAQUS

5.1 Introduction

ABAQUS is a suite powerful engineering simulation programs, based on the finite element method that can solve problems ranging for relatively simple linear analyses to the most challenging nonlinear simulations. ABAQUS contains an extensive library of elements that can model virtually any geometry. It has an equally extensive list of material models that can simulate the behavior of most typical engineering materials including metals, rubber, polymers, composites, reinforced concrete, crushable and resilient foams, and geotechnical materials such as soils and rock. Designed as a general-purpose simulation tool, ABAQUS can be used to study more than just structural (stress/displacement) problems. It can simulate problems in such diverse areas as heat transfer, mass diffusion, thermal management of electrical components (coupled thermal-electrical analyses), acoustics, soil mechanics (coupled pore fluid-stress analyses), and piezoelectric analyses.

ABAQUS is simple to use even though it offers the user a wide range of capabilities. The most complicated problems can be modeled easily. For example, problems with multiple components are modeled by associating the geometry defining each component with the appropriate material models. In most simulations, even highly nonlinear ones, the user need only provide the engineering data such as the geometry of the structure, its material behavior, its boundary conditions, and the loads applied to it. In nonlinear analyses, ABAQUS automatically chooses appropriate load increments and convergence tolerances. Not only does it choose the values for these parameters, it also continually adjusts them during the analyses to ensure that an accurate solution is obtained efficiently. The user rarely has to define parameters for controlling the numerical solution of the problem.

5.2 The ABAQUS Modules

ABAQUS consist of two main analyses modules: ABAQUS/Standard and ABAQUS/Explicit. There are also two special-purpose add-on analyses products for ABAQUS/Standard: ABAQUS /Aqua and ABAQUS/Design. In addition ABAQUS /Safe provides fatigue postprocessing; while ABAQUS/ADAMS, ABAQUS/CAT, ABAQUS/C-MOLD, and ABAQUS/MOLDFLOW are interfaces to ABAQUS/Flex, CATİA, C-MOLD, and MOLDFLOW respectively. BAQUS/CAE is the complete ABAQUS environment that includes capabilities for creating ABAQUS modes, interactively submitting and monitoring ABAQUS jobs, and evaluating results. ABAQUS/Viewer is a subset of ABAQUS/CAE that includes just the postprocessing functionally.

5.2.1 ABAQUS/Standard

ABAQUS/Standard is a general-purpose analyses module that can solve a wide range of linear and nonlinear problems involving the static, dynamic, thermal, and electrical response of components.

5.2.2 ABAQUS/Explicit

ABAQUS/Explicit is a special-purpose analyses module that uses an explicit dynamic finite element formulation. It is suitable for short, transient dynamic events, such as impact and blast problems, and is also very efficient for highly nonlinear problems involving changing contact conditions, such as forming simulations. The ABAQUS/CAE interface is the same for both analyses module. In addition, the output is similar for the two modules, and ABAQUS/Viewer can be used to postprocess the results from either module.

5.2.3 ABAQUS/CAE

ABAQUS/CAE (Complete ABAQUS Environment) is an interactive, graphical environment for ABAQUS. It allows model to be created quickly and easily by producing or importing the geometry of the structure to be analyzed and decomposing the geometry into meshable regions. Physical and material properties can be assigned to the geometry, together with loads and boundary conditions. ABAQUS/CAE contains very powerful options to mesh the geometry and to verify the resulting analyses model. Once the model complete, ABAQUS/CAE can submit, monitor, and control the analyses jobs. The Visualization module can then be used to interpret the results.

5.2.4 ABAQUS/Viewer

ABAQUS/Viewer is the Visualization module of ABAQUS/CAE; it is an interactive, graphical postprocessor that supports all of the capabilities in the ABAQUS analyses modules and provides a wide range of options for interpreting the results.

5.2.5 ABAQUS/Aqua

ABAQUS/Aqua is a set of optional capabilities that can be added to ABAQUS/Standard. It is intended for the simulation of offshore structures, such as oil platforms. Some of the optional capabilities include the effect of wave and wind loading and buoyancy.

5.2.6 ABAQUS/ADAMS

ABAQUS/ADAMS allows ABAQUS finite element models to be included as flexible components within the MDI ADAMS family of products. The interface is based on the component mode formulation of ADAMS/Flex.

5.2.7 ABAQUS/CAT

ABAQUS/CAT allows ABAQUS analyses to be set up and postprocessed entirely in CATIA.

5.2.8 ABAQUS/C-MOLD

ABAQUS/C-MOLD translates finite element mesh, material property, and initial stress data from C-MOLD mold filling analysis to an ABAQUS input file.

5.2.9 ABAQUS/Design

ABAQUS/Design is a set of optional capabilities that can be added to ABAQUS/Standard to perform design sensitivity calculations.

5.2.10 ABAQUS/MOLDFLOW

ABAQUS/MOLDFLOW translates finite element model information from a MOLDFLOW analyses to write a partial ABAQUS input file.

5.2.11 ABAQUS/Safe

ABAQUS/Safe is the fatigue analyses module in ABAQUS. Using results from ABAQUS analyses, it determines the fatigue life of a component.

5.3 The 3D model design in ABAQUS

First of all the pull plate specimen‘s 3D modal is designed in ABAQUS. All dimensions are in metric system in this designing.

5.4 Modeling of the Pull-Plate Specimen

In this study, pull-plate specimen is modeled using ABAQUS preprocessor. Figure 5.1 shows the three dimensional solid model of the welded structure. This model is the simplifying model of the beam-to-column connection.

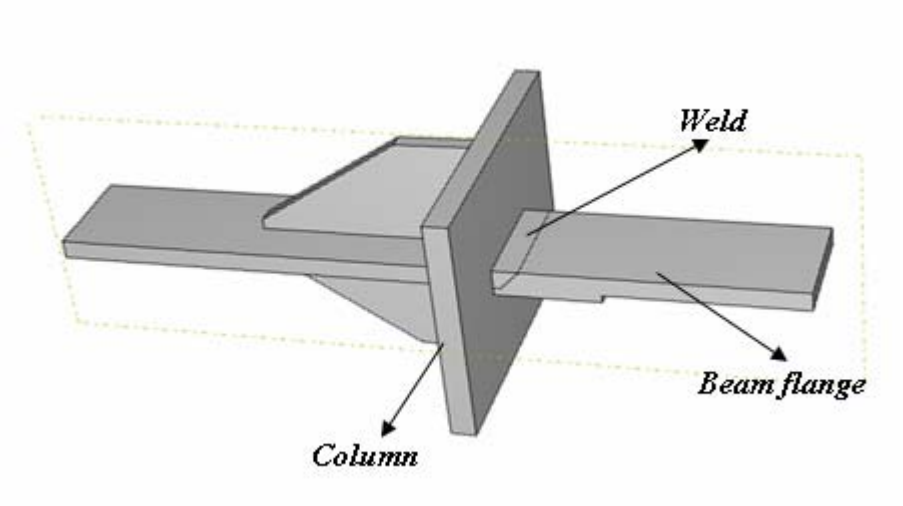

Figure 5.1 Three dimensional solid model of the pull-plate specimen

The plate which is front face of the column is 300 mm height and 30 mm thickness. Sketch of the column face is shown in Figure 5.2

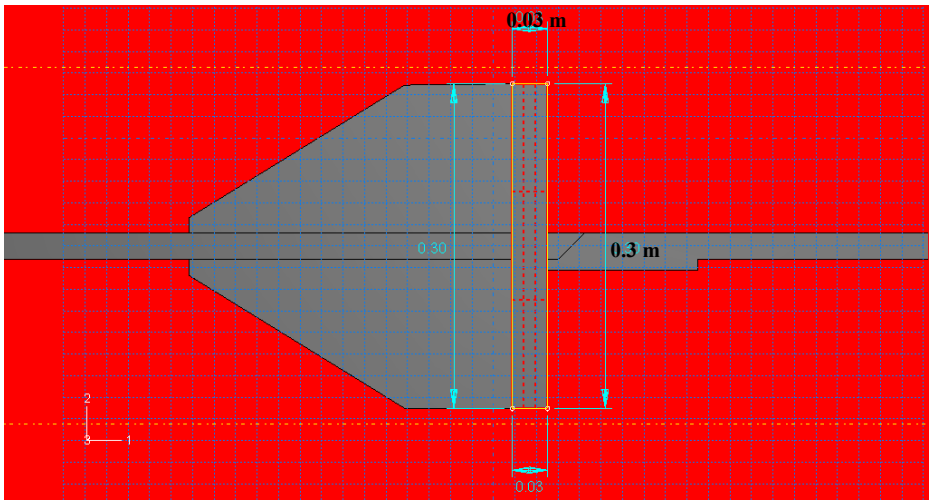

Figure 5.2 The section sketch of model and dimensions.

The crack type chosen to represent the defect must be relatively close to real defects in structures. Therefore, the initial defect is modeled as a semi-elliptical surface crack (EC3, 1995). The crack is assumed to be planar. Furthermore, since the defect size is small compared to the size of a structural element, it is assumed that the plate dimensions are infinite. The crack is defined by its length, *a*, and shape *a/c*, where is half crack surface width (AWS, 2000).

In this dissertation, semi-elliptical surface crack is placed through the heat-affected zone at the connection where the column flange meets the bottom flange of the beam as shown in Figure 5.3.

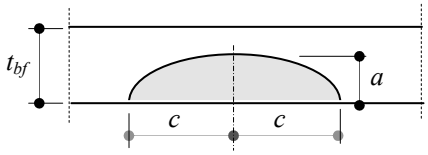

Figure 5.3 Geometry of the initial defect chosen a semi-elliptical surface crack in an infinite plate (AWS, 2000)

The crack section's geometry and dimensions are given in Figure 5.4.

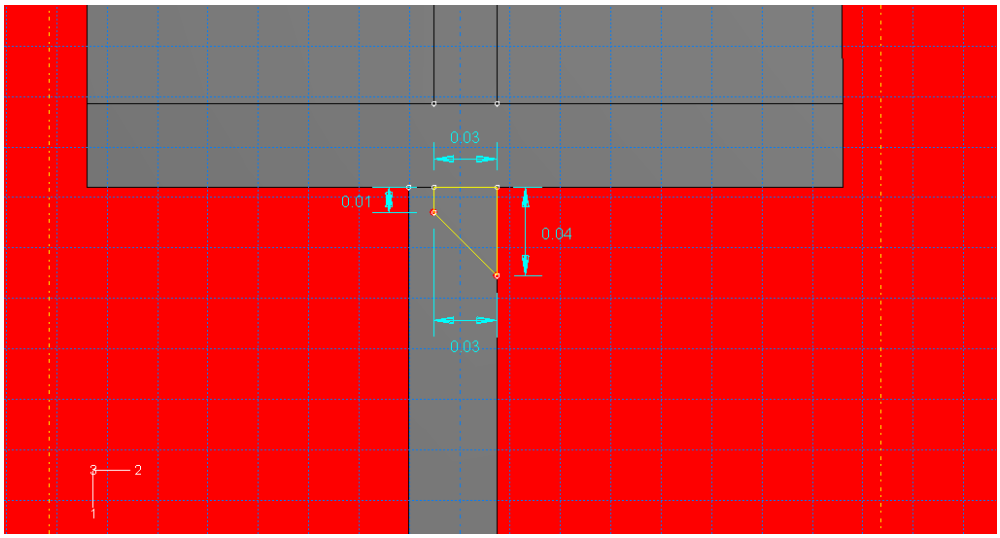

Figure 5.4 Crack model and dimensions

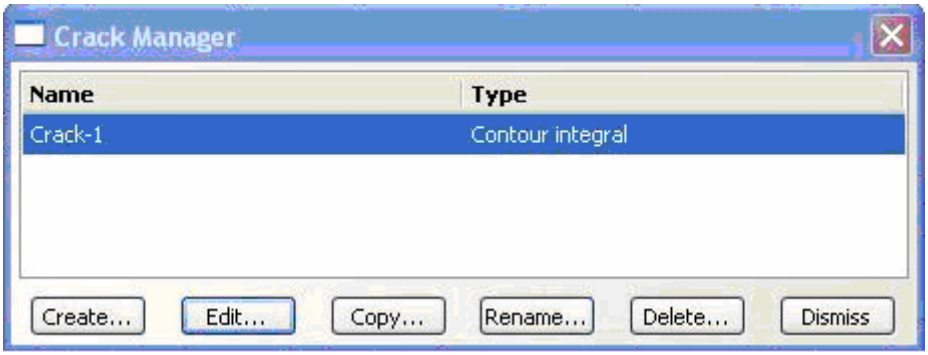

Figure 5.5 Crack manager

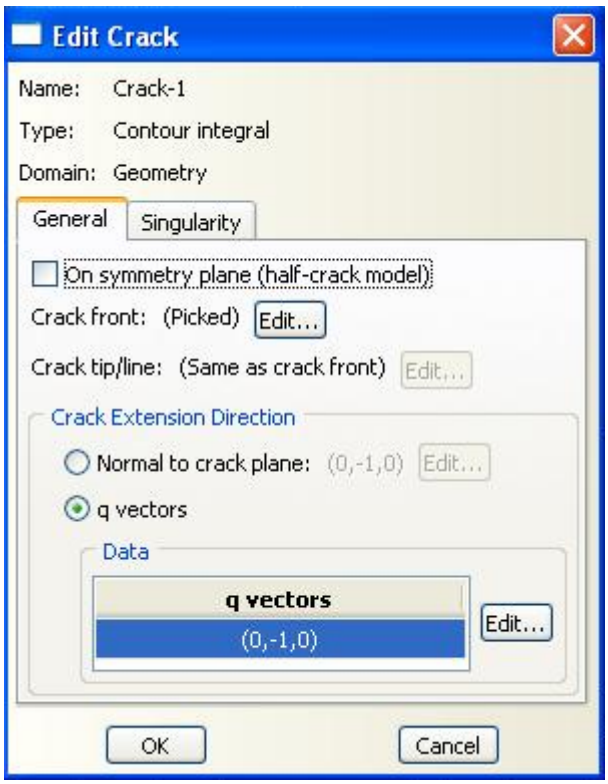

Figure 5.6 Edit crack window

After modeling, material properties should be identified. In order to determine the effects of the electrode type on the fracture behavior of the welded structure, four different weld materials are used in the finite element analyses. Since the elastic-plastic analyses are performed, full strain-stress curve should be defined. The material characteristic properties that include density, elastic and plastic material properties are written in the Property Step.

Beam and column are both A 572 steel Gr. 50, weld materials are E7018, E70TG-K2, E70T-6 and E71T-8 electrodes in order to see the effects of the electrode type.

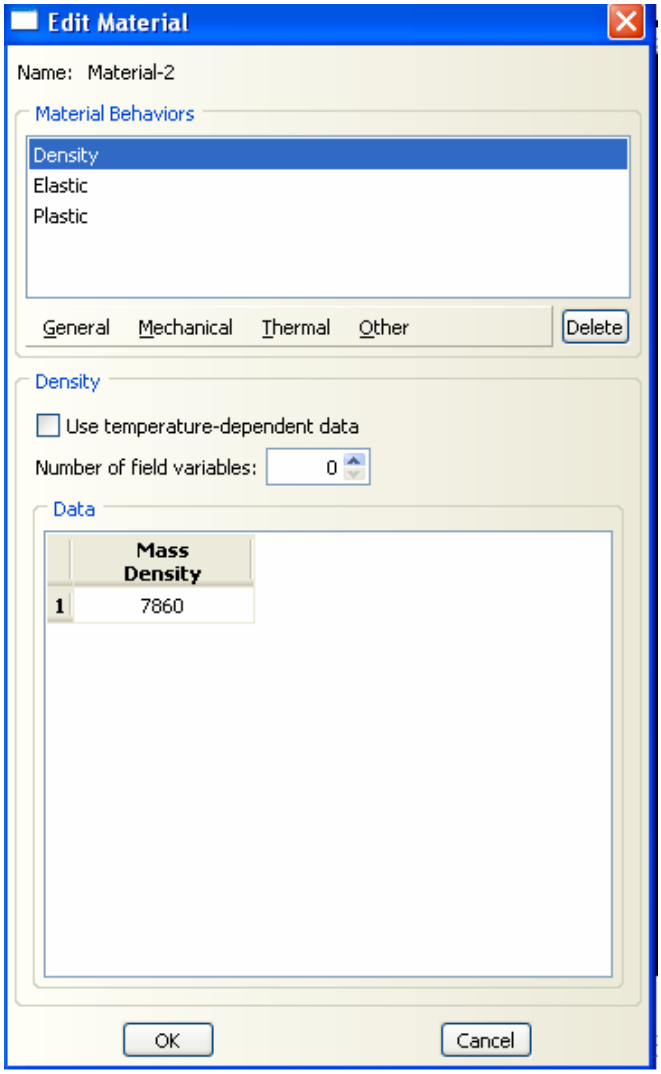

Figure 5.7.a The material properties window

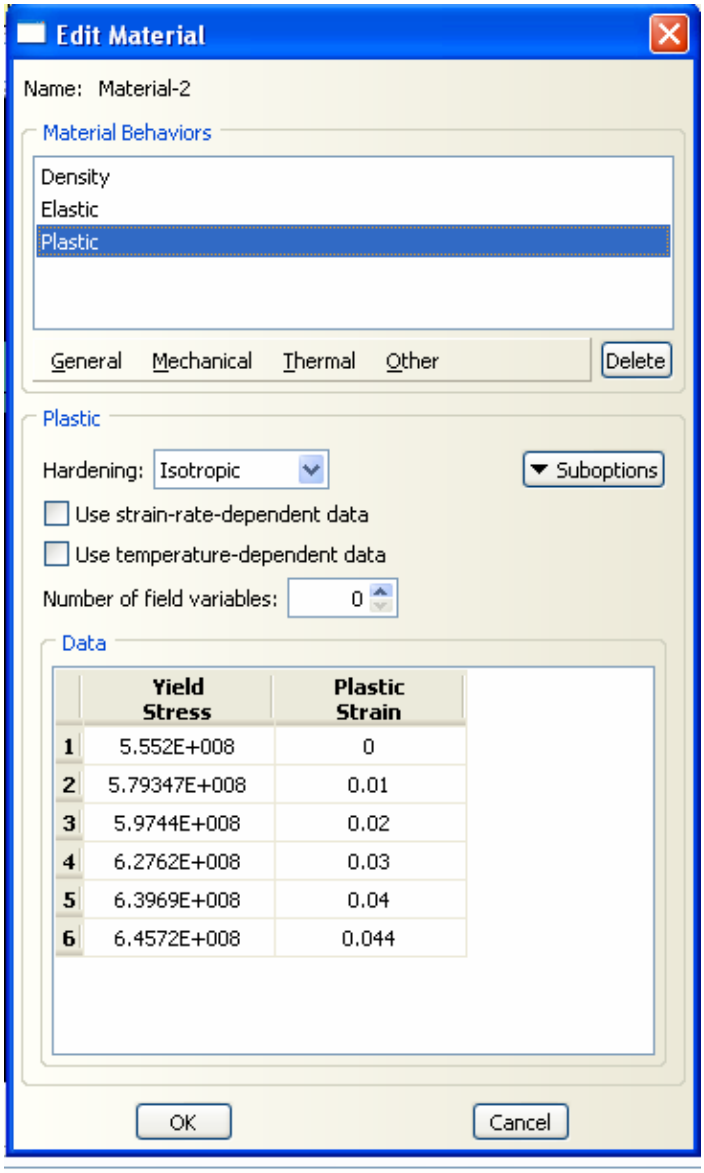

Figure 5.7.b The material properties window

The crack is created in the Interaction module. The crack region is shown in Figure 5.8.

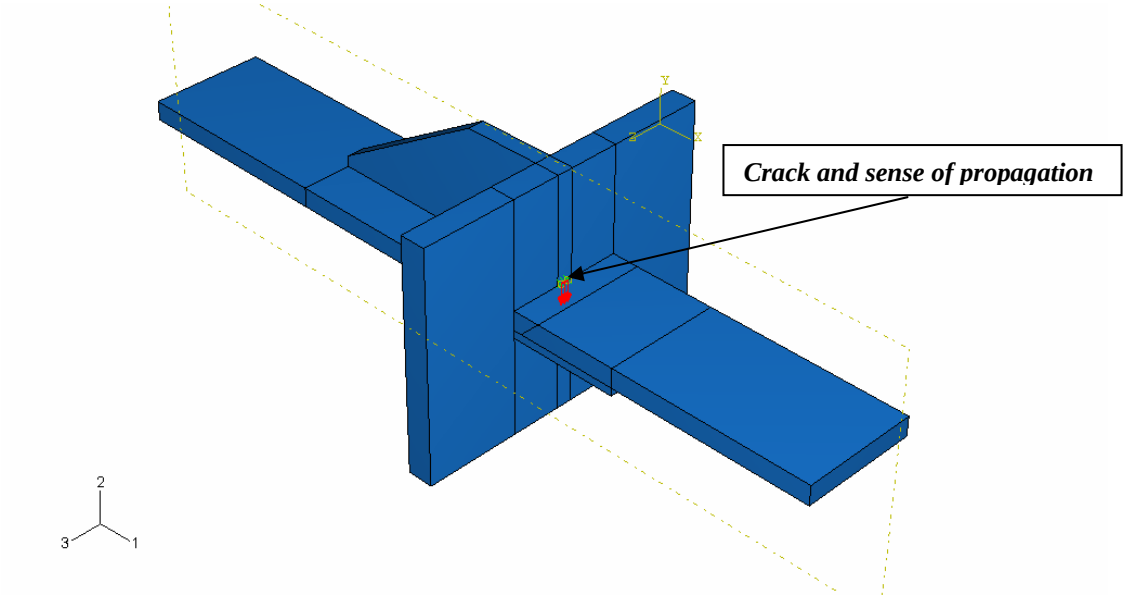

Figure 5.8 Crack model

The boundary conditions like forces and displacement are defined in the Load Step module. They are shown in Figure 5.9. Tensile load is applied to the beam. Column is supported as clamped boundary condition.

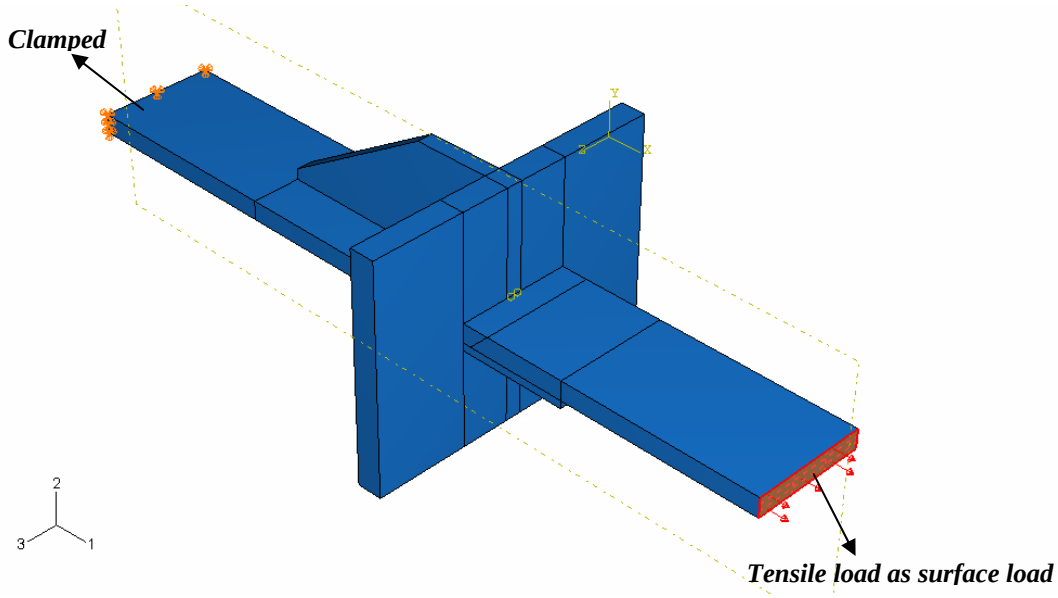

Figure 5.9 Boundary conditions

Figure 5.10 shows the finite element model of the pull-plate specimen. The finite element model includes 3240 C3D8R elements (8-node linear brick hexagonal elements).

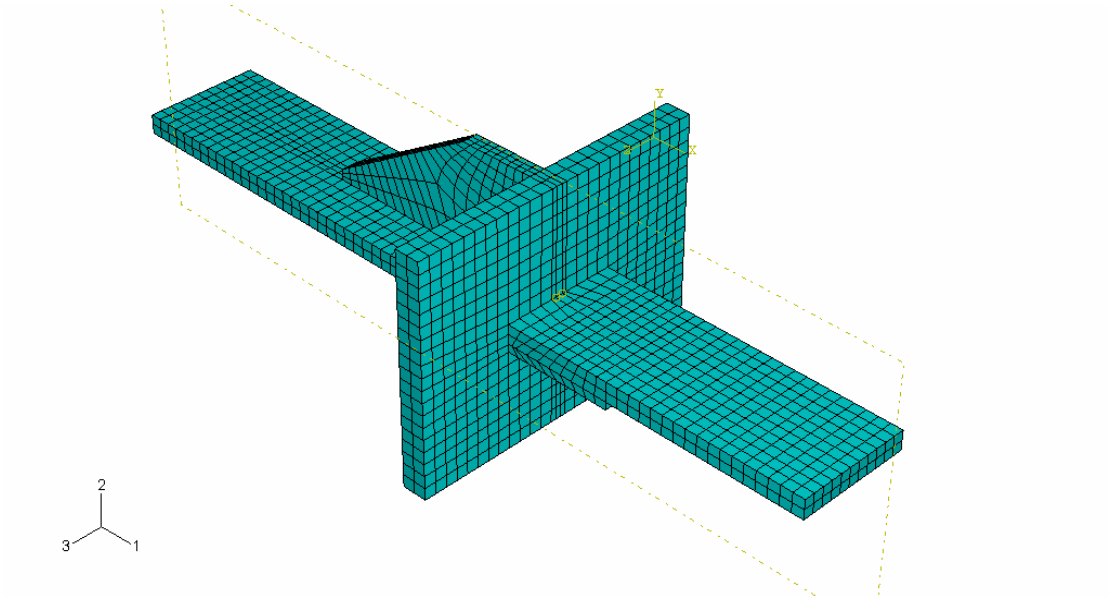

Figure 5.10 Finite element model of the pull-plate specimen

CHAPTER SIX
RESULTS

In this thesis, the fracture behavior of the welded steel structures has been examined. The effect of the electrode type has been explored by using ABAQUS 6.5 software based on the elastic-plastic finite element method. Pull-plate specimen has been used simplifying the column-beam connection. The specimen has an elliptical surface in the weld region. The von-Mises stresses, the maximum principal stresses and J-integral values under static and dynamic loads have been determined.

6.1 Static Analyses

The effect of four electrode types is examined on the fracture behaviors of pull-plate specimen. Three different tensile loads are applied to the beam surface. These are 450 MPa (2025 kN), 150 MPa (625 kN) and 45 MPa (202.5 kN). After having completed the analyses, von-Misses stresses, maximum principal stresses (σ_1) and J-integral values are determined.

Table 6.1 shows the fracture toughness values of the base and weld metals. As shown, the most tough weld metal is E7018.

Table 6.1 Fracture toughness values of base and weld metals (Chi, 1999)

Material	CVN_s (J)	CVN_d (J)	K_{Ic} (MPa $\sqrt{m}$)	$CTOD_c$ (mm)	J_c (N/mm)
A572	266	266	252	0.47	293.56
E70T6	68	50	100	0.041	39.39
E70TG-K2	120	98	120	0.078	68.11
E70T8	250	109	140	0.121	97.41
E7018	197	185	204	0.307	268.06

Due to expense and size limitations associated with fracture toughness tests, it is useful to make estimations of fracture toughness from CVN toughness requirements.

The empirical correlation between CVN and K_{IC}, fracture toughness, is as follows (Motarjemi & Koçak, 2002):

$$K_{IC} = \sqrt{\frac{E\left(0.53CVN^{1.28}\right)\times 0.2^{\left(0.133CVN^{0.256}\right)}}{1000\left(1-\upsilon^2\right)}} \tag{6.1}$$

where K_{IC} in MPa$\sqrt{\text{m}}$ and CVN in Joule.

K_{IC} can be also converted $CTOD_C$,

$$K_{IC} = \sqrt{m \cdot \sigma_{flow} E \cdot CTOD} \tag{6.2}$$

where for plane-strain problem m=1.6 (Broek, 1989) and σ_{flow} is the average of yield strength and ultimate strength, $\sigma_{flow}=(\sigma_y+\sigma_u)/2$ is flow stress (Chi, 1999).

Correlation between CTOD and J-integral energy is as follows,

$$J_c=m\cdot\sigma_{flow}\cdot CTOD \tag{6.3}$$

Table 6.2 The static analyses results

	450 MPa			**150 MPa**			**45 MPa**		
	J-int (N/mm)	**σ_{VM} (MPa)**	**σ_1 (MPa)**	**J-int (N/mm)**	**σ_{VM} (MPa)**	**σ_1 (MPa)**	**J-int (N/mm)**	**σ_{VM} (MPa)**	**σ_1 (MPa)**
E7018	1.75E+05	515.2	719.1	196.24	193	211.9	17.66	57.9	61.38
E70T6	1.73E+05	579.7	718.9	196.24	193	211.9	17.66	57.9	61.38
E70T8	3.35E+05	529.9	719.1	196.24	193	211.9	17.66	57.9	61.38
E70TG-K2	3.33E+05	550.8	719.1	196.24	193	211.9	17.66	57.9	61.38

Table 6.2 presents the numerical results obtained by the static finite element analyses. As seen from the table, under 45 MPa, the specimen is in the elastic region. In this condition, although maximum stress value is not bigger than the yield

strength, J-integral value show that the unexpected fracture may be occur due to the presence of the crack in the structure. Since the elasticity modulus values of all weld materials are same, so the stresses and J-integral values in the structure do not change. Applying 150 MPa, J-integral is 196.24 N/mm although von-Mises stress is 193 MPa. Except E7018, J_c values of all weld materials are less than 196.24 N/mm. It can be said that brittle fracture occurs since von-Mises stress is lower than the yield strength.

The plastic deformation occurs in the structure under 450 MPa because the von-Mises stress is higher than the yield strength for all electrode types. The largest stress value occurs when E70T6 electrode type is used. It is seen from the table that J-integral is very large. These results show that the failure is unavoidable in case of the presence of the crack.

Variation of J-integral, von-Mises and maximum principle stresses are given Figure 6.1.a, b and c, respectively. As shown in Figure 6.1.a, minimum J-integral value occurs when E7018 and E70T6 electrodes are used in the welded structure.

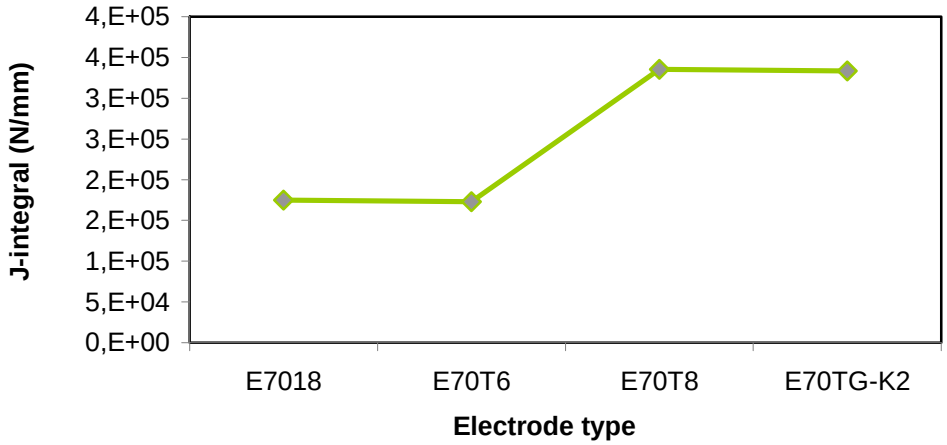

Figure 6.1.a The J-integral values versus electrode types

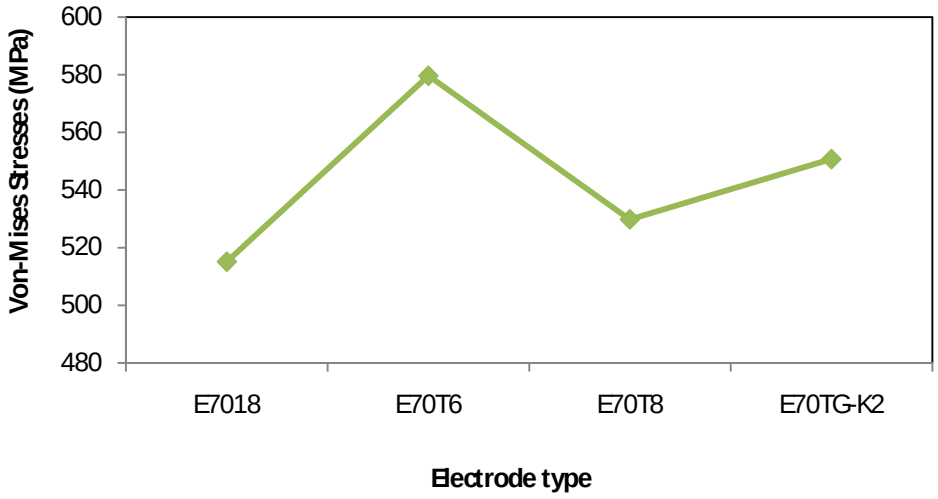

Figure 6.1.b Von-Mises stress values versus electrode types

Figure 6.1.b shows the effect of the electrode type on the variation of von-Mises stress. Minimum von-Mises stress value occurs when E7018 electrode type is used.

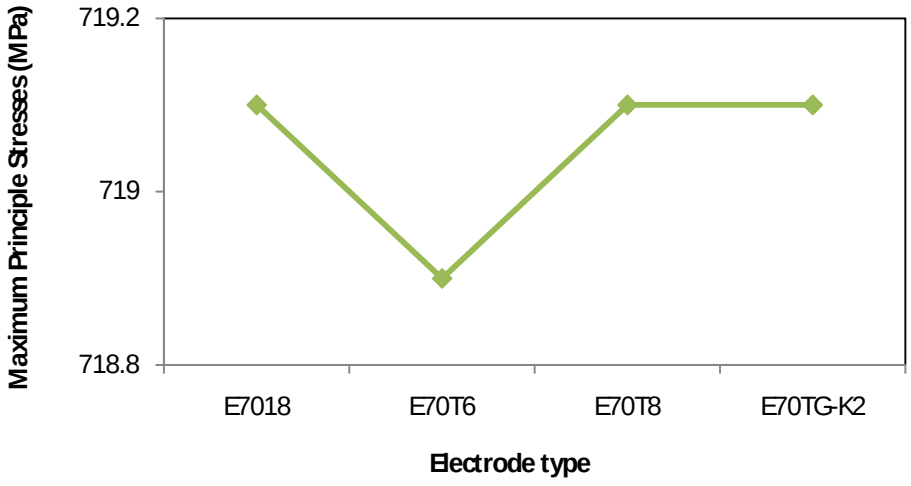

Figure 6.1.c Maximum Principle Stresses values of Electrode Types

Figure 6.1.c shows the variation of maximum principle stress according to electrode type. This stress component results in propagation of the crack. As shown in the figure, stress values for all electrodes are close. This result indicates the fracture toughness value of the weld material very important designing the welded structures prone to earthquakes.

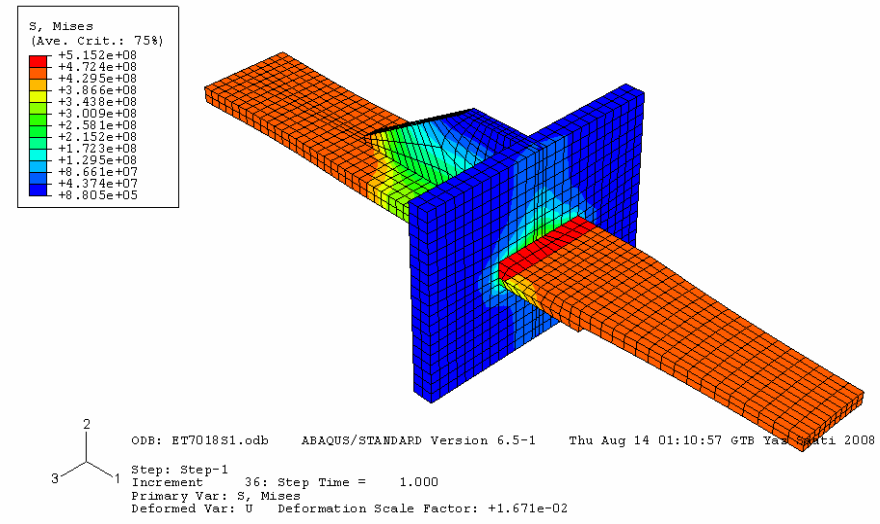

Figure 6.2.a Von-Mises stress distribution for E7018 (450 MPa)

Von-Mises stress distribution in pull-plate specimen under static loads is shown in Figure 6.2.a. As seen from the figure, von-Mises stress increases in crack region.

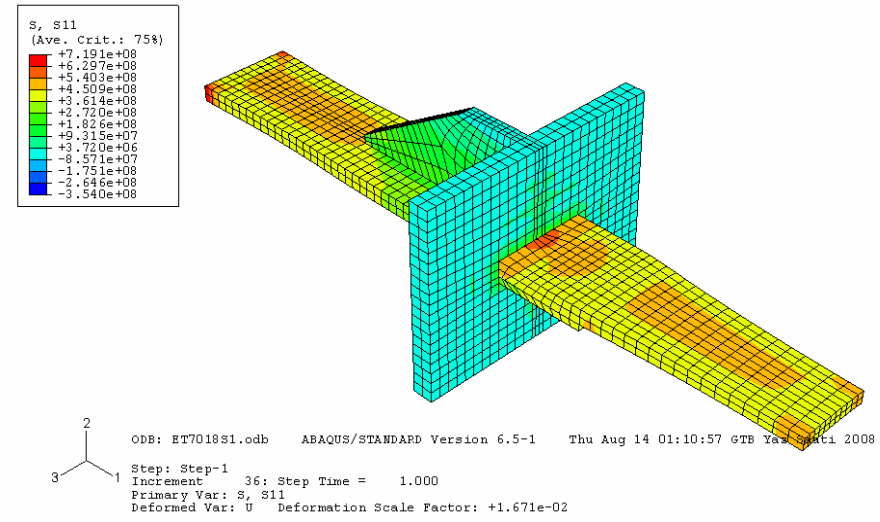

Figure 6.2.b Maximum principle stress distribution for E7018 (450 MPa)

Maximum principle stress distribution in pull-plate specimen under static loads can be seen in Figure 6.2.b. As seen from the figure, maximum principle stress increases in crack region. This component of stress may cause the fracture.

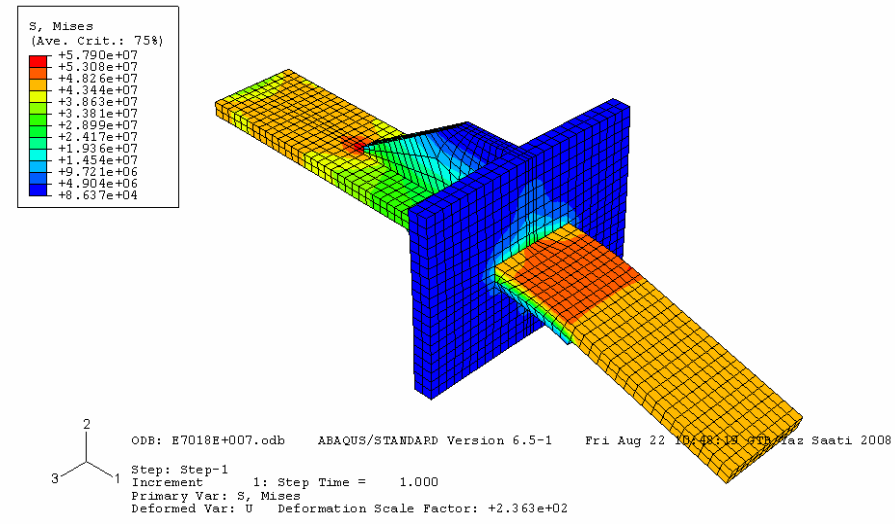

Figure 6.3.a Von-Mises stress distribution for E7018 (45 MPa)

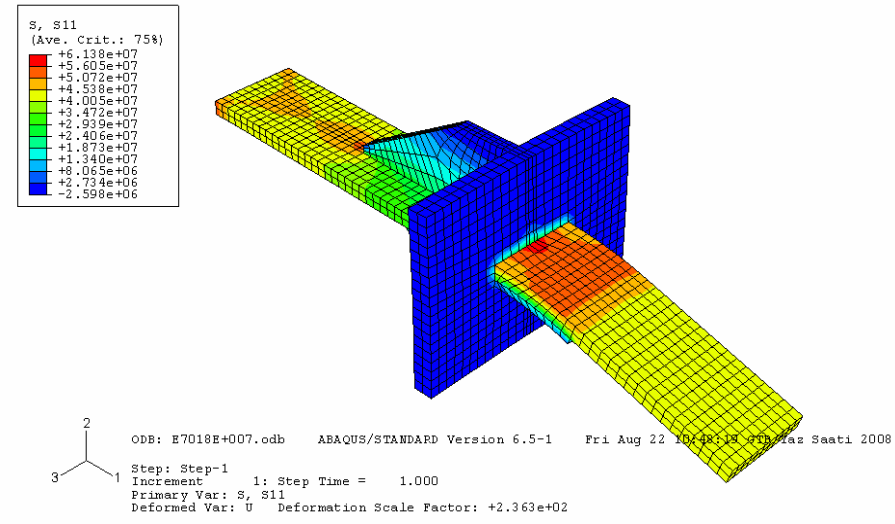

Figure 6.3.b Maximum principle stress distribution for E7018 (45 MPa)

Von-Mises and maximum principle stresses distributions in pull-plate specimen under static load (45 MPa) for E7018 are shown in Figure 6.3.a and b.

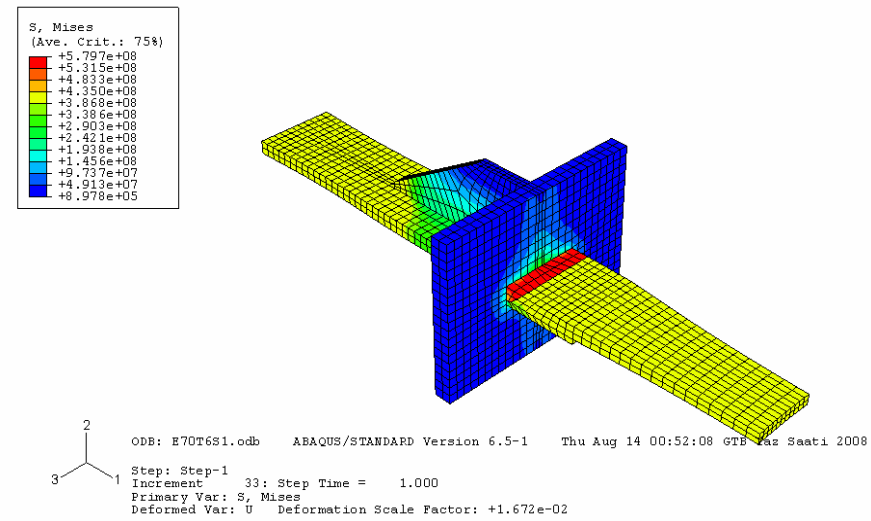

Figure 6.4.a Von-Mises stress distribution for E70T6 (450 MPa)

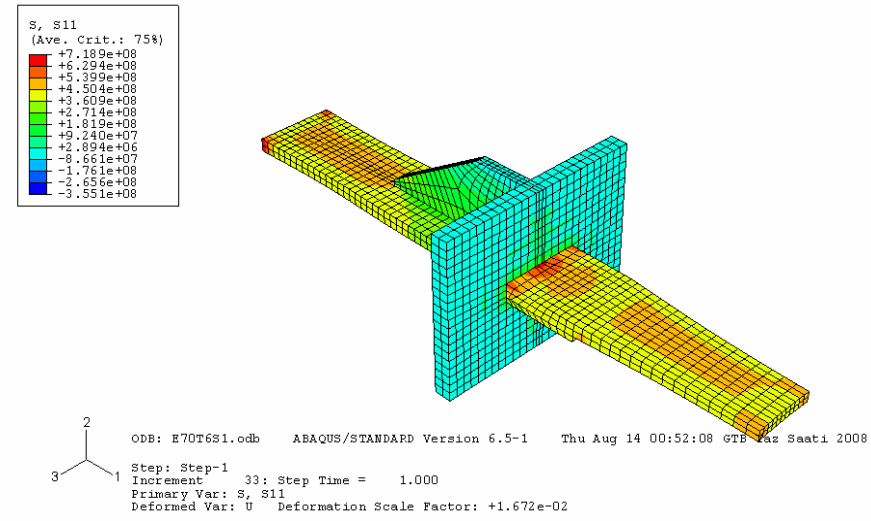

Figure 6.4.b Maximum principle stress distribution for E70T6 (450 MPa)

Von-Mises and maximum principle stresses distributions in pull-plate specimen under static load (450 MPa) for E70T6 are shown in Figure 6.4.a and b.

6.2 Dynamic Analyses

Civil engineering structures are always designed to carry their own dead weight, superimposed loads and environmental forces such as wind or waves. These loads are usually treated as maximum loads not varying with time and hence as static loads. In some cases, the applied load involves not only static components but also contains a component varying with time which is a dynamic load. In the past, the effects of dynamic loading have often been evaluated by using an equivalent static load, or by an impact factor, or by a modification of the factor of safety. Structures where it is particularly important to consider dynamic loading effects are construction of tall buildings, long bridges under wind-loading conditions and buildings in earthquake zones, etc (Kuntiyawichai & Burdekin, 2003).

In this section, dynamic analyses in time-domain are performed to examine the dynamic effects on the strength and fracture behavior of the welded steel structure. Dynamic analyses are made for frequency values of 1 Hz, 2 Hz and 2.5 Hz as shown in Figure 6.5. Earthquake is low frequency phenomenon. Seismic loading is defined as the loading, which occurs in building structures due to ground motions varying with time at frequencies in a band up to 15 Hz with most damage in a band up to about 3 Hz. The ground motions may produce horizontal and/or vertical accelerations and the response of the structure depends on its natural frequencies of vibration in relation to the dominant frequencies of the earthquake and on the magnitude of the earthquake (IIW, 2002).

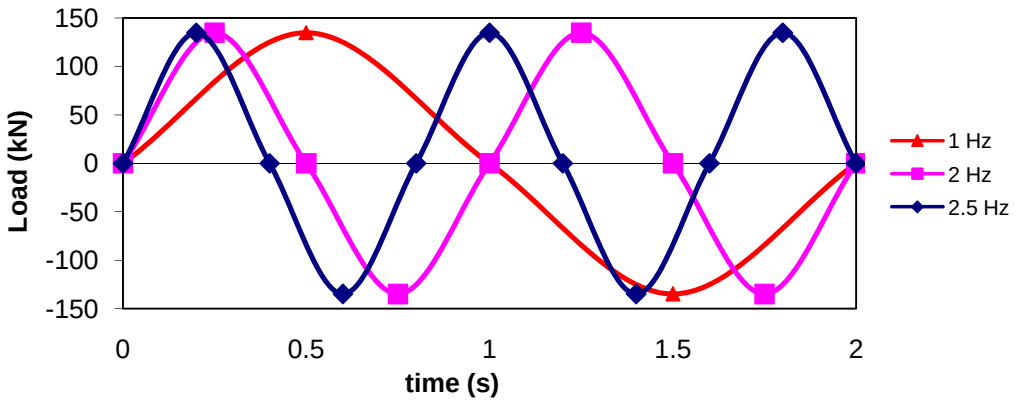

Figure 6.5 Transient loads acting on the welded steel structure

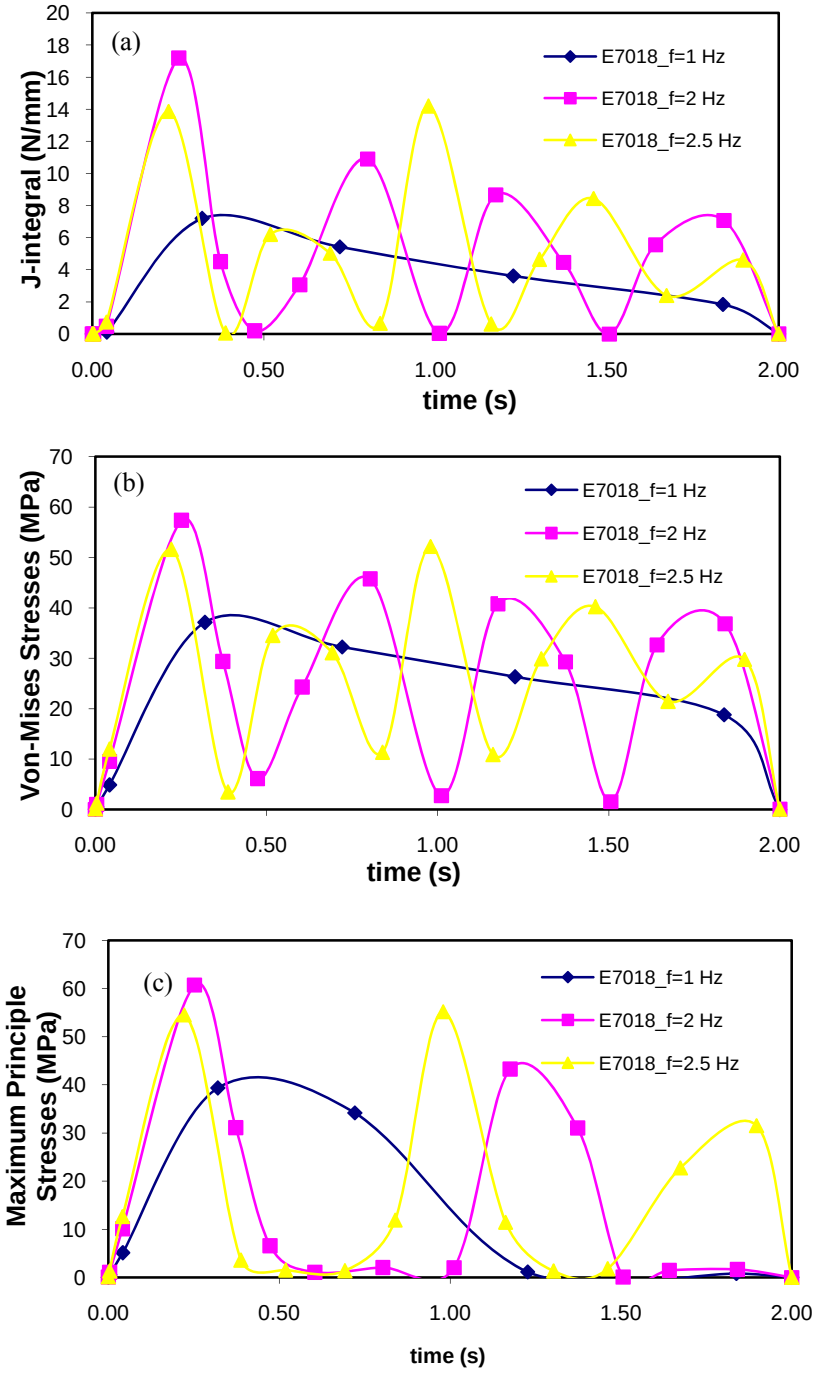

Figure 6.6 Variation of a) the J-integral, b) von-Mises stresses and c) maximum principle stresses versus time for E7018

Figure 6.6 shows the effect of the forcing frequency on the J-integral, von-Mises stresses and the maximum principal stresses for E7018. As shown in the figure, at the 2 Hz, they reach maximum values. These values are close to results of static analyses.

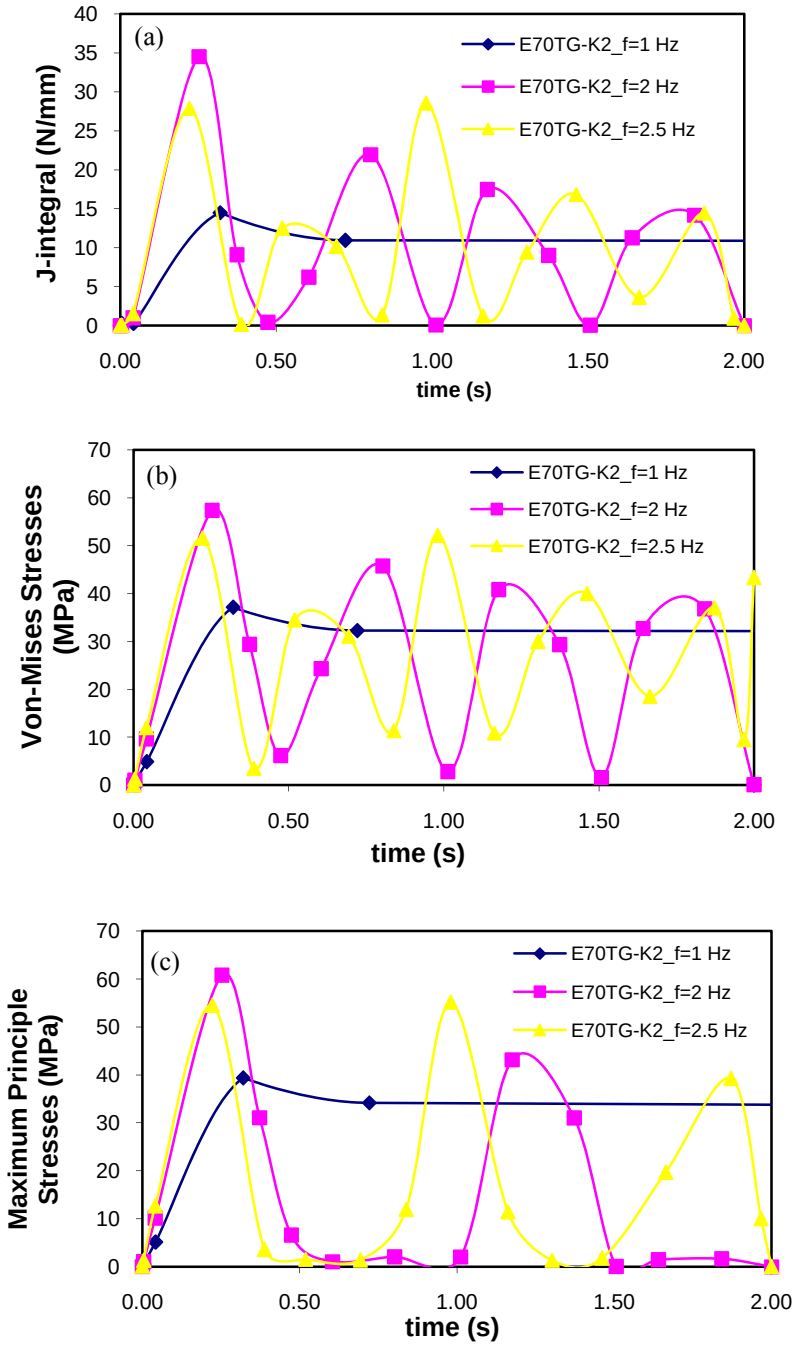

Figure 6.7 Variation of a) the J-integral, b) von-Mises stresses and c) maximum principle stresses versus time for E70TG-K2.

Figure 6.7 shows the effect of the frequency of the load on the J-integral, von-Mises stresses and the maximum principal stresses for E70TG-K2. At the 2 Hz, they reach maximum values.

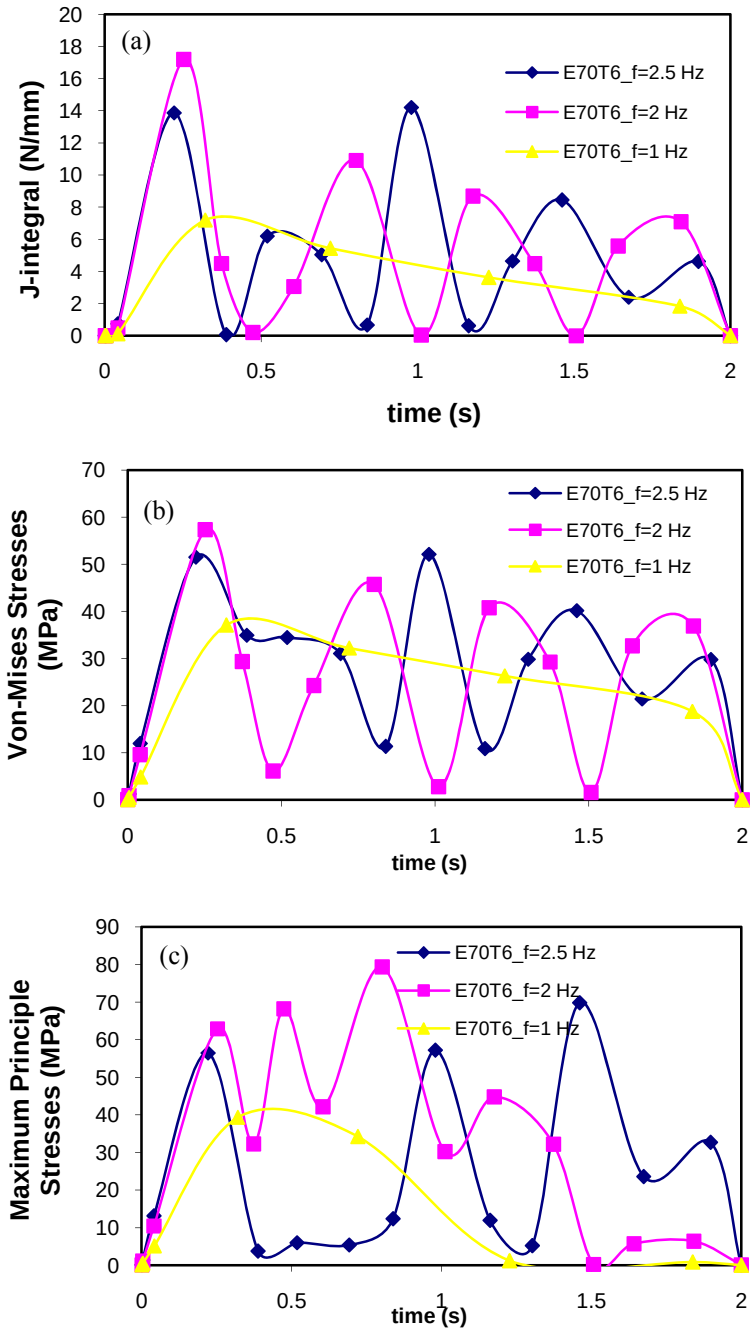

Figure 6.8 Variation of a) the J-integral, b) von-Mises stresses and c) maximum principle stresses versus time for E70TG-K2.

Figure 6.8 shows the effect of the frequency of the load on the J-integral, von-Mises stresses and the maximum principal stresses for E70T6. J-integral and von-Mises stresses are close to results of static analyses. However, maximum principle stress value is bigger than that obtained by the static analysis.

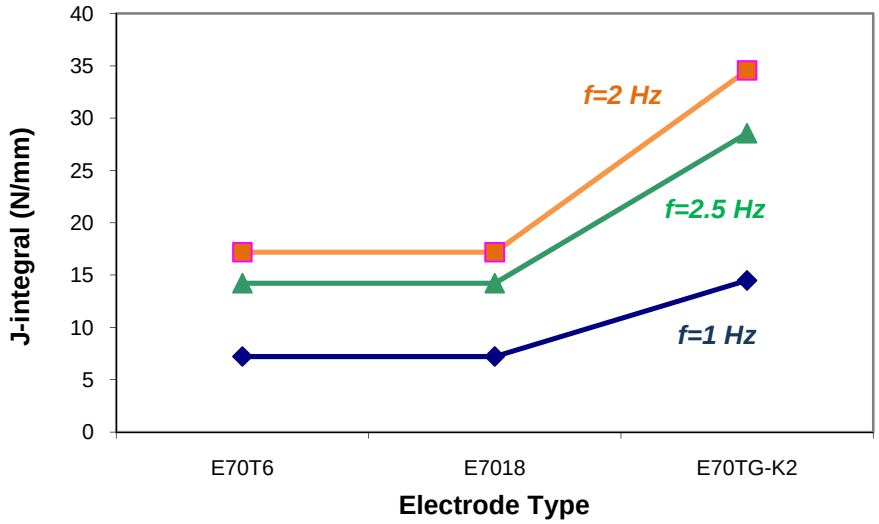

Figure 6.9 J-integral values versus forcing frequency

Figure 6.9 summarizes the effects of the forcing frequency and electrode types on the fracture behavior of the welded structures. As seen in the figure, maximum J-integral values occur at 2 Hz with use of E70TG-K2 electrode.

CHAPTER SEVEN
CONCLUSIONS

The aim of this thesis is to develop the steel welded beam-to-column connections subjected to earthquake loads and examine the effects of the strain rate, presence of the crack, material properties on the performance of the structure.

The stress-strain and fracture behaviors of the pull-plate specimen under the static and dynamic loads are investigated by using the nonlinear finite element method. The effects of the forcing frequency on the overall structural strength are also examined.

From the results presented in this thesis, the following points of discussion are summarized:

- The presence of the crack increases the probability of the brittle fracture.
- The failure may occur even if state of the stress is in elastic region.
- Stress increases in the crack region because of the stress concentration due to the geometrical discontinuities.
- In unloading case, residual stresses at the crack tip increase as the forcing frequency increases because there is no enough time for relaxation.
- Tough weld electrode should be used in the welded steel structure, especially prone earthquake.

REFERENCES

Ainsworth, R. A., Bannister, A. C. & Zerbst U. (2002). *An Overview of the European Flaw Assessment Procedure SINTAP and Its Validation*. Int. J. Press. Vessels and Piping, 77, 869-876.

Ainsworth, R. A., Guiterrez-Solana, F. & Ocejo, J. R. (2000). Analysis levels in the SINTAP defect assessment procedures. *Engineering Fracture Mechanics*, 67, 515-527.

Allen, J., Partridge, J., Radau, S. & Richard, R. (1998). Ductile connection designs for welded steel moment frames, *Proceedings of the Conf. on Welded Construction in Seismic Areas, Hawaii.*

Anderson, T.L. (1995). *Fracture Mechanics, Fundamentals and Applications.* USA: CRC Press.

Azuma, K., Kurobane, Y. & Makino, Y. (2000). Cyclic testing of beam-to-column connections with weld defects and assessment of safety of numerically modeled connections from brittle fracture. *Engineering Structures*, 22, 1596-1608.

Bonowitz, D. & Youssef, N. (1995). Steel moment-resisting frames after Northridge, *Modern Steel Construction*, May, 46-55.

Broberg, K.B. (1999). *Cracks and Fracture.* United Kingdom, Cambridge: Academic Press.

Bruneau, M. (2000). USA Preliminary report on Marmara, Turkey earthquake, *MCEER Multidisciplinary Center for Earthquake Engineering Research*, University of Buffalo.

Burdekin, F.M & Suman, A. (2000). *Further thoughts on the relationship between toughness, workmanship and design for earthquake resistant structures*, AWS reports, 14 March.

Calado, L. & Azevedo, J. (1989). *A model for predicting the failure of structural steel elements*, J. Construct. Steel Research, 14, 41-64.

Chi, W.M. (1999). *Prediction of steel connection failure using computational fracture mechanics*. Ph. D. Thesis. Stanford University.

Clifton, G.C., Butterworth, J.W. & Scholz, W. (1998). *Performance of rigid welded beam to column joints under inelastic cyclic loading, Proceedings of the Conf. on Welded Construction in Seismic Areas*, Hawaii.

Engelhardt, M.D. & Sabol, T.A. (1996). Lessons learned from Northridge earthquake: Steel moment frame performance. *Symposium on a New Direction in Seismic Design*, Tokyo, Japan.

Fisher, J., Dexter, R.J. & Kaufmann, E.J. (1998). *Fracture mechanics of welded structural steel connections, Proceedings of the Conf. on Welded Construction in Seismic Areas*, Hawaii.

F.M. Burdekin, M. Toyoda, M. Huther, C.S. Wiesner. (2000). *Brittle fracture risk assessment procedure for seismically affected steel structures.* Florida, American Welding Society.

F.M. Burdekin. (2000). *Further thoughts on the relationship between toughness, workmanship and design for earthquake resistant structures.* Florida, American Welding Society.

F. Minami, T. Hashida, M. Toyoda, T. Ohmura, K. Arimochi & N. Konda. (1998). *Prediction of dynamic fracture toughness from static toughness results.* Hamburg, International Institute of Welding (IIW).

Hao, S. Brocks, W. & Schwalbe, K-H. (1996). A procedure to estimate the limit load of a tensile panel with surface crack, *ASME Offshore Mechanics and Arctic Engineering Conference (OMAE 96)*, Florence, 16-20 June.

Irwin, G.R. (1977). *Fracture Mechanics*. New Jersey: Prentice-Hall, Inc.

Kim, Y-J. & Schwalbe, K. H. (2001). Mis-match effect on plastic yield loads in idealised weldments I. Weld centre cracks*, Engineering Fracture Mechanics*, 68, 529-546.

Kim, Y-J. & Schwalbe, K. H. (2001). Mis-match effect on plastic yield loads in idealised weldments II. Heat Affected Zone Cracks*, Engineering Fracture Mechanics*, 68, 529-546.

Koçak, M. & Motarjemi, A. K. (2002). Structural integrity of advanced welded structures. *IIW Int. Conf. on Advanced Processes and Technologies in Welding and Allied Processes*, Copenhagen, Denmark.

Kuntiyawichai, K. & Burdekin, F.M. (2003). Engineering assessment of cracked structures subjected to dynamic loads using fracture mechanics assessment, *Engineering Fracture Mechanics,* 70, 1991-2014.

Lei Y. and Ainsworth R.A. (1997). *The estimation of J in three-point-bend specimens with a crack in a mismatched weld*. Int. J. Pres. Ves. & Piping, 70, pages 247-257.

Marin J. (1966). *Mechanical Behavior of Engineering Materials*. New Delphi: Prentice-Hall, Inc.

Matos, C.G. & Dodds, R.H. (2001). Probabilistic modeling of weld fracture in steel frame connections part I: *quasi-static loading, Engineering Structures*, 23, 1011-1030.

Matos, C.G. & Dodds, R.H. (2001). Probabilistic modeling of weld fracture in steel frame connections part II: *seismic loading, Engineering Structures*, 24, 687-705.

Motarjemi, A. K. & Koçak, M. (2002). Fracture assessment of a clad steel using various SINTAP defect assessment procedure levels, *Fatigue Fracture&Engineering Material Structure*, 25, 929-939.

M. Toyoda. (1997). *Effect of strain rate under seismic loading on fracture behaviors of welded structures*. San Francisco, International Institute of Welding.

M. Toyoda. (1997). *Lessons learned by failure examples in great Hanshin earthquake*. San Francisco, International Institute of Welding.

Murakami, Y. (1987). *Stress Intensity Factors Handbook*. Oxford: Pergamon Press.

Nakagomi, T., Yabe, Y., Fujita, T., Ohbayashi, Y. & Lee., K. (1998). Study on details of column-to-beam connections against earthquake*, Proceedings of the Conf. on Welded Construction in Seismic Areas*, Hawaii, October.

Paterson, S., Vaillancourt, H. & Kuntz, T. (1998). Variability and statistical bounds of the strength and fracture toughness of common structural steel shapes and welded metals used in welded steel moment frame connections in building construction, *Proceedings of the Conf. on Welded Construction in Seismic Areas*, Hawaii.

Popov, E., Amin, N.R., Louie, J.J.C. & Stephen, R.M.. (1985). Cyclic behavior of large beam-column assemblies, *Earthquake Spektra*, 1, 203-238.

Rahman, S. & Wilkowski, G. (1998). Net-Section-Collapse analysis of circumferentially cracked cylinders-Part I: Arbitrary-shaped cracks and generalized equations, *Engineering Fracture Mechanics*, 61, 191-211.

Rahman, S. (1998). Net-Section-Collapse analysis of circumferentially cracked cylinders-part II: arbitrary-shaped cracks and generalized equations, *Engineering Fracture Mechanics*, 61, 213-230.

Righiniotis, T. D., Omer, E. & Elghazouli, A. Y. (2002). A simplified crack model for weld fracture in steel moment connections, *Engineering Structures*, 24, 1133-1140.

Scawthorn, C. (2000). Preliminary Report on Kobe, Japan, *MCEER Multidisciplinary Center for Earthquake Engineering Research.*

Scholz, W., Diekman, A. & Schere, J. (1998). Low cycle, high strain rate, inelastic performance of welded, moment-resisting connections, *Proceedings of the Conf. on Welded Construction in Seismic Areas*, Hawaii.

Shimanuki, H., Yoyoda, M. & Hagiwara, Y. (1998). Fracture mechanics analysis of damaged steel framed structures in recent earthquakes, *Proceedings of the Conf. on Welded Construction in Seismic Areas*, Hawaii.

Suita, K. & Tada, M. Full-scale tests to determine plastic rotation capacity of steel wide-flange beams connected with square tube columns, *Proceedings of the Conf. on Welded Construction in Seismic Areas*, Hawaii.

Thaulow C., Ranestad O., Hauge M., Zhang Z., Toyoda M. and Minami F. (1997) FE calculations of stress fields from cracks located at the fusion line of weldments. *Engineering Fracture Mechanics*. 57 (6), pages 637-651.

T. Nakagomi, Y. Yabe, T. Fujita, I. Ohbayashi, Y. Sasaki & K. Lee. (1997). *Study on details of beam to column welded connection to exert on the earthquake resistance capacity of steel structures*. San Francisco, International Institute of Welding.

T. Nakagomi, S. Minami, Y. Ichikawa, I. Ohbayashi, M. Oka & K. Lee.(1997). *Effect of the repeating of the strain rate, the axial force, the plastic strain on the fracture of beam-to-column welded connection.* San Francisco International Institute of Welding.

T.Nakagomi, M. Fujimoto, A. Hirofumi, J.Nishizawa & I. Ohbayashi. (1997). *The brittle fracture of the beam-to column connection in consideration of the mechanical property of the structural steel and the weld metal*. San Francisco, International Institute of Welding (IIW).

Toyoda, M. (1995). How steel structures fared in Japan' s great earthquake. *Welding Journal*, 74, 12-42.

Toyoda, M. (1997). Problems related to materials for avoiding failure of steel framed structures under heavy earthquake, *IIW JWG on Brittle Fracture*, Paris.

Y. Kurobane. (1997). Brittle fracture in steel building frames. *Comparative study of Northridge and Kobe earthquake damage*. San Francisco, International Institute of Welding.

Y. Kurobane, B. Wang, K. Azuma & K. Ogawa. (1997). *Brittle fracture in steel frames*. San Francisco, International Institute of Welding.

Y. Kurobane. (1998). *Evaluation of importance factors influencing deformation capacity of steel moment connections*. Hamburg, International Institute of Welding.

Wang, B., Kurobane, Y. & Makino, Y., Structural safety assessment to welded T joints under combined tensile and bending loads, *Proceedings of the 8th Symposium on Fracture Mechanics*, 1995.

Webster S. & Bannister, A. (2000). Structural integrity assessment procedure for Europe of the SINTAP program overview, *Engineering Fracture Mechanics*, 67, 481-514.

Xiao D. and Dexter R.J. (1998) Finite element calculations of applied J-integral for cracked ship structural details. *Engineering Fracture Mechanics*. 60 (1), pages 59-82.

Xue, M., Kaufman E.J., Lu, L.W. & Fisher J.W. (1996). Achieving ductile behavior of moment connections-Part II, *Modern Steel Construction*, June, 38-42.

APPENDICES

List of Tables

Page

List of Figures

Page